1992-06

Numerical analysis of the flow in a turbulated rectangular duct simulating the cooling passages in a turbine blade

Palatka, Robert M.

Monterey, California. Naval Postgraduate School

Approved for public release; distribution is unlimited.

Numerical Analysis of the Flow in a Turbulated Rectangular Duct Simulating the Cooling Passages in a Turbine Blade

by

Robert M. Palatka
Lieutenant , United States Coast Guard
B.S., United States Military Academy
M.S., University of Southern California

Submitted in partial fulfillment
of the requirements for the degree of

MASTER OF SCIENCE IN AERONAUTICAL ENGINEERING

from the

NAVAL POSTGRADUATE SCHOOL
June, 1992

REPORT DOCUMENTATION PAGE

1a. REPORT SECURITY CLASSIFICATION Unclassified	1b. RESTRICTIVE MARKINGS
2a. SECURITY CLASSIFICATION AUTHORITY	3. DISTRIBUTION/AVAILABILITY OF REPORT Approved for public release; distribution is unlimited.
2b. DECLASSIFICATION/DOWNGRADING SCHEDULE	
4. PERFORMING ORGANIZATION REPORT NUMBER(S)	5. MONITORING ORGANIZATION REPORT NUMBER(S)
6a. NAME OF PERFORMING ORGANIZATION Naval Postgraduate School 6b. OFFICE SYMBOL *(If applicable)* 55	7a. NAME OF MONITORING ORGANIZATION Naval Postgraduate School
6c. ADDRESS *(City, State, and ZIP Code)* Monterey, CA 93943-5000	7b. ADDRESS *(City, State, and ZIP Code)* Monterey, CA 93943-5000
8a. NAME OF FUNDING/SPONSORING ORGANIZATION 8b. OFFICE SYMBOL *(If applicable)*	9. PROCUREMENT INSTRUMENT IDENTIFICATION NUMBER
8c. ADDRESS *(City, State, and ZIP Code)*	10. SOURCE OF FUNDING NUMBERS Program Element No. / Project No. / Task No. / Work Unit Accession Number

11. TITLE *(Include Security Classification)*
Numerical Analysis of the Flow in a Turbulated Rectangular Duct Simulating the Cooling Passages in a Turbine Blade

12. PERSONAL AUTHOR(S) Robert M. Palatka

13a. TYPE OF REPORT	13b. TIME COVERED	14. DATE OF REPORT *(year, month, day)*	15. PAGE COUNT
Master's Thesis	From To	1992 June 15	93

16. SUPPLEMENTARY NOTATION
The views expressed in this thesis are those of the author and do not reflect the official policy or position of the Department of Defense or the U.S. Government.

17. COSATI CODES			18. SUBJECT TERMS *(continue on reverse if necessary and identify by block number)*
FIELD	GROUP	SUBGROUP	Turbulator, Computational Fluid Dynamics, Heat Transfer, Grid, Duct,

19. ABSTRACT *(continue on reverse if necessary and identify by block number)*

An extensive review of the literature revealed that many experimental studies have been conducted in heat-transfer wind tunnels simulating the cooling passages in turbine blades. However, very few numerical studies have been performed. Phoenics, a computational fluid dynamics computer program, produced results for several duct configurations and calculated the heat transfer characteristics of each. The configurations investigated included a straight, square duct and a rectangular duct with turbulators, (a form of turbulence promoters) present. The parameters varied included Reynolds numbers, turbulence intensity and grid geometry. Results for the turbulated duct indicated highly distinct and repeatable flow patterns developed over a wide range of values. The variation of the inlet turbulence intensity had little impact on the kinetic energy. The results proved to be highly grid dependent, which greatly impacted the correlation between experimentally and numerically produced data, for the same configurations, under similar operating parameters.

20. DISTRIBUTION/AVAILABILITY OF ABSTRACT	21. ABSTRACT SECURITY CLASSIFICATION	
☒ UNCLASSIFIED/UNLIMITED ☐ SAME AS REPORT ☐ DTIC USERS	Unclassified	
22a. NAME OF RESPONSIBLE INDIVIDUAL Garth V. Hobson	22b. TELEPHONE *(Include Area code)* (408) 646-2888	22c. OFFICE SYMBOL AA HG

DD FORM 1473, 84 MAR — 83 APR edition may be used until exhausted. All other editions are obsolete — SECURITY CLASSIFICATION OF THIS PAGE: Unclassified

ABSTRACT

An extensive review of the literature revealed that many experimental studies have been conducted in heat-transfer wind tunnels simulating the cooling passages in turbine blades. However, very few numerical studies have been performed. Phoenics, a computational fluid dynamics computer program, produced results for several duct configurations and calculated the heat transfer characteristics of each. The configurations investigated included a straight, square duct and a rectangular duct with turbulators (a form of turbulence promoters) present. The parameters varied included Reynolds numbers, turbulence intensity and grid geometry. Results for the turbulated duct indicated highly distinct and repeatable flow patterns developed over a wide range of values. The variation of the inlet turbulence intensity had little impact on the kinetic energy. The results proved to be highly grid dependent, which greatly impacted the correlation between experimentally and numerically produced data, for the same configurations, under similar operating parameters.

TABLE OF CONTENTS

I. INTRODUCTION

A. BACKGROUND TO TURBINE INTERNAL COOLING

All modern gas turbine engines share three basic components; the compressor, the combustion chamber and the turbine. From the compressed mainstream flow out of the combustion chamber the turbine extracts the power to operate the compressor and to deliver the gases to either a power turbine for shaft work or to a nozzle for thrust. During this process losses occur in both the compressor and the turbine sections. In the compressor they serve to increase the power absorbed while in the turbine they act to decrease the power output. To overcome these losses, more air and therefore fuel flow are required for a required power level. The compressor loss increases the temperature of the flow out of the compressor and into the combustor and decreases the amount of fuel which can be added for a given turbine inlet temperature. Based on cycle analysis, the higher the allowable temperature into the turbine the higher the power output of the unit. The turbine inlet temperature constrains the design of all gas turbine engines.

Thus for a given engine, the amount of fuel which the fuel control unit (FCU) can add is limited by the ability of the materials to withstand thermal loads. Failures can result

from effects such as oxidation, corrosion and erosion, as well as creep (due to a combination of thermal and centrifugal loads) and fatigue, which ensues from both thermal and cyclic loads. The combination of these effects determine the operating life of the turbine. Two solutions to this problem have emerged. One is the improvement of materials for the construction of turbine components, the other is the use of compressor bleed air to cool the turbine components.

Turbine blade cooling will be discussed in the following order: external cooling air over turbines, impingement cooling, film cooling, transpirational cooling and with the final focus on internal cooling using turbulators. Experiments in turbine cooling began in the 1940's with the first units going into operation around 1960. Initial engines bled 1.5 to 2 % of the compressed air from the compressor to cool the turbine 200-300° C [Ref 1]. Modern aircraft engines can use as much as 20% of the compressor discharge flow [Ref 2]. This cooling air externally bathes the turbine blade with initial rotors receiving their cooling air directly from the compressor discharge. Two shortcomings associated with this type of cooling include the turbine's reduced ability to drive the compressor because of the lower temperature of the flow as it enters the turbine and the mixing of the cooling and the mainstream flow that results in increased aerodynamic losses.

Rather than just providing external cooling air, individual cooling of the airfoil itself is another attempt to elevate turbine inlet temperatures. Impingement cooling at the leading edge and at midchord consists of placing a sheet metal insert into the hollow turbine blade with appropriately placed venting holes. Coolant flows through the root of the blade into the insert and out the impingement holes. This convective type cooling directs air at the hottest spots on the blade and creates airflow inside the blade. Often the most difficult part of the design analysis involves determining the exact location of the stagnation point or hottest spot on the blade. After the cooling process occurs the blade vents the coolant either at the tip or at the trailing edge, which then joins the main flow.

Film cooling also uses air from the compressor routed into the root of the blades. In film cooling this air travels through the blade and departs through openings designed to produce a blanket of cooling air to protect the blade against the mainstream gases. The analysis on the design of these holes focuses on number, location, size, shape and orientation angle. With the average cooling effectiveness (ACE) defined as;

$$\phi = \frac{T_{tg} - T_m}{T_{tg} - T_c} \qquad (1)$$

where T_{tg} is the mainstream gas total temperature, T_m is the average surface temperature of the airfoil and T_c is the coolant supply total temperature, engineers usually specify film cooling for an ACE of 0.6. Film cooling is very effective when combined with other forms of internal convective cooling, but the price in total pressure losses for putting such a quantity of cooling air into the hotter main gas flow is considerable.

Another form of cooling is transpirational or aspiration cooling. This technique uses a porous material to construct the airfoil and runs cooling airflow into and through it. This combines both convective and film cooling, but with some obvious problems associated with the strength of the airfoil construction. Designers using a woven wire material achieved some success, however difficulties in the shaping of the airfoils may preclude this type of construction.

The final type of cooling discussed is internal cooling passages with coolant run through the blade and out at the tip and trailing edge of the blade. Only convective cooling is used and chosen when the design calls for an ACE of less than 0.5. Internal designers choose convective cooling because of a limited supply pressure (a higher ACE would require a higher pressure), and a higher effectiveness level using just convective cooling could lead to a higher temperature gradient and thus aggravate the very thermal stress problem which cooling tries to avoid.

B. EXPERIMENTAL INVESTIGATIONS

Investigations into internal passages for convective heat transfer fall into three sub-areas; straight passages, serpentine passages with one or more 180° bends and single and multi-pass channels undergoing rotation. The investigations often include analysis of different flow properties, channel shapes, aspect ratios and wall roughness, which encompasses the shape, location, number and orientation of turbulence inducing structures. The continual refinement of the operating characteristics of turbine engines has made this last characteristic increasingly important as many of the other parameters are fixed.

As early as the 1960's research centered on the effects of protrusions into the flow from the walls of the channel. Wilkie [Ref 3] was one of the first to publish results of experimentation on the effects of rib roughened ducts on heat transfer. The interest in cooling operations in nuclear reactor fuel elements resulted in the findings he collected and published. Through variations in duct equivalent diameter (d), rib height (e) and rib pitch or spacing (p) he found correlations between the Stanton number, the Reynolds number, the p/e ratio and the e/d ratio. The Stanton number is defined as $h/(u\rho C_p)$ where h is the heat transfer coefficient, u is the velocity in the free stream at the outer edge of the boundary layer, ρ is the fluid density and C_p is the specific heat at constant pressure. The results showed Stanton number

varied less with Reynolds number for small values of e/d (<.012), and behaved much as on a smooth surface at larger values of e/d (>.012). In addition he found the value of the p/e ratio giving maximum Stanton numbers varied with e/d and Reynolds number but tended to approximately the value six at large e/d irrespective of Reynolds number. Norris [Ref 4] also detailed the effect of these "turbulators" in his investigation. After testing various shapes, he concluded that although the local heat-transfer coefficient varied in a very non-uniform manner in the stream-wise direction, there was a value of the pitch-to-width ratio for the square turbulator which gave an optimum value for the average heat transfer as well as friction factor. Increasing the ratio above this level served only to decrease these values. Also, he developed a relationship between the friction factor of his test apparatus and the friction factor of a smooth duct, and found an optimum value existed for this ratio. Increases above this value did not give increased heat transfer.

Using the Nusselt number as an indicator of heat transfer, Han, et. al. [Ref 5] varied their rib angle (α) and spacing to determine their effects. With a rib-to-height ratio of ten, they found the Nusselt number to be twice as high with the turbulators placed 90° to the flow as for the case without turbulators. Introducing an α of 60° increased the Nusselt number another 5% while an α of 45° delivered an additional 25% over the 90° orientation. Lau, et. al. [Ref 6] built upon

this concept when they examined fully developed flow in a square channel with turbulence promoters on two opposed walls, using turbulators configured with α's of 45°, 60° and 90°, lengths running from wall to wall, and shorter discrete turbulators. Both configurations were tested, crossed or parallel with respect to each other. They found parallel discrete ribs with α's of 60° provided the highest ribbed wall heat transfer, while the same style of ribs canted at 30° provided the lowest level of pressure drop. In general they recommended using parallel, angled discrete ribs for internal cooling passages as they provided higher ribbed wall heat transfer, lower smooth wall heat transfer and lower channel pressure drop. The optimum configuration for these discrete ribs was a continually staggered row pattern of three ribs followed by a row of two ribs.

Taslim and Spring [Ref 7] centered their straight square channel experiments not so much on the placement of the turbulators, but rather the geometry of them. They determined that an optimum turbulator spacing existed for every given turbulator blockage ratio and aspect ratio. The turbulator blockage ratio was defined as the ratio of the turbulator height to the hydraulic diameter of a non-turbulated section. They also found that the Nusselt number decreased as the turbulator aspect ratio decreased. This became even more critical as the spacing dropped below the optimum value. They also developed an alternatively shaped turbulator which not

only provided the same heat transfer performance as a larger turbulator, but also enhanced the castability and, thus, reduced the probability of problems in manufacturing. To do this they developed a turbulator with a narrow tip width to enhance flow while at the same time widening the base to ease the problems of castability. The resulting shape is trapezoidal with slightly rounded corners at the tip.

Prior to Boyle's [Ref 8] report, most data for turbulators came from experiments using long passages with measurements done in regions where results did not change with distance. Boyle initiated his report with an investigation of a serpentine channel without any turbulators. He researched the effect of bends only on heat transfer coefficients. He found that when varying the outside edge of the turn from square to a round geometry he did not alter the heat transfer rate. He established that the rate varied directly proportional to the Reynolds number and the highest rate occurred at the beginning of the second leg after the bend. The addition of turbulators markedly increased the heat transfer rate. He also found an optimum height which required the turbulator to extend into the boundary layer buffer region.

Chandra, et. al. [Ref 9] did additional work on a multi-pass serpentine channel investigating the effect of the turbulator angles on the flow. Using a ratio of average Sherwood numbers normalized to Sherwood numbers for fully developed turbulent flow, they equated this value to the

ratios of average Nusselt numbers normalized with respect to Nusselt numbers for fully developed turbulent flow. Here they define the Sherwood number (Sh) as:

$$Sh = \frac{h_m D_h}{\nu S_c} \qquad (2)$$

where h_m is the local mass transfer coefficient or the local mass transfer rate per unit area divided by the difference of the coolant density at the wall and freestream; D_h is the hydraulic diameter, ν is the kinematic viscosity and S_c is the Schmidt number for the coolant. The Schmidt number is the ratio of the kinematic viscosity to the mass diffusivity. Using the above equation they were able to make a heat to mass transfer analogy. For the straight channel they found periodic Sherwood numbers on the ribbed walls in the direction of flow, while α's of 60° and 45° produced higher Sherwood numbers on the outer walls than on the inner ones. Turbulators set perpendicular to the flow produced little spanwise variation of heat transfer, and the slight spanwise variations they did find diminished somewhat after the 180° turns. In general they found that with respect to the area of the turn the overall average Sherwood number ratio was independent of the rib angle but tended to decrease slightly as the Reynolds number increased.

Using a three-pass rib-roughened channel Han and Zhang [Ref 10] established the local pressure drop distribution.

With these data, they were able to determine the local coolant flow rate distribution. Their results indicated that the pressure dropped linearly for the first leg to the turn. Just prior to the turn, a slight rise followed by a sharp drop occurred into, through and just after the bend. Flow recirculation caused a recovery of pressure during the second straight channel, with a similar pressure drop occurring at the second turn. They also found the turbulators' biggest impact to be evident in the first straight channel prior to the turn. The 180° turns tended to dilute their impact on subsequent legs.

Chyu [Ref 11] did similar testing with both two- and three-pass channels employing 180° turns. The emphasis of these experiments was on surface heat transfer coefficient versus pressure distribution. With the two-pass channel, he found that while the pressure loss attributable to the turn was significant, it was independent of the Reynolds number. His findings of flow separation, reattachment, impingement and secondary flows caused by the 180° turn are consistent with the findings of Han and Zhang. He attributed the heat transfer levels observed to be due to these secondary flow effects. Also, even though he found the heat transfer rates of both turns to be approximately equal, the total heat transfer of a three pass channel was about 15% greater than for a two pass channel.

With a three-pass square channel, with two 180° turns, Han and Zhang [Ref 12] investigated the impact of angling turbulators 60° on opposite walls. They also opted for mass transfer to be the measured experiment parameter and converted to Sherwood numbers to correlate the heat transfer. Configuring the ribs both crossed and parallel to the opposite wall, they found α's of 60° produced greater mass transfer coefficients than α's of 90°, while parallel ribs generated greater coefficients than crossed ones. Starting with a smooth channel, they established the value of the second leg's mass transfer to be 60% greater than the first leg. Since the third leg closely approximated the second, they surmised that the 180° turn caused the difference. Finding, in general, the 60° parallel orientation provided the highest mass transfer coefficients, this study showed rib angle orientation plus sharp turns in the coolant path can increase or decrease the mass transfer coefficient. In addition, by correlating previous data with the results of this experiment, they validated the application of straight ribbed channel data to the first pass in multi-pass ribbed cooling channels.

The final area of investigation associated with internal convective cooling of turbine blades relates to rotating elements. Clifford [Ref 13] used a rotating, three pass, smooth channel with airflow directed through it. Measuring the heat transfer along the leading and trailing walls with respect to rotation, he found rotation served to both aid and

inhibit heat transfer with the reductions approaching 30% on the suction side of the final leg and the enhancement closer to 35% on the pressure side of the initial leg. Averaging his data showed the effects of rotation reduced the heat transfer to 90% of the statically measured values.

Morris and Harasgama [Ref 14] performed similar tests using axial airflow directed both radially inward and outward. Their results showed outwardly directed airflow promoted greater cooling on the trailing (pressure) surface vice the leading (suction) surface. Inwardly directed airflow, however, increased heat transfer on the leading surface. This heat transfer was rotational Reynolds number dependent as it increased slightly as the number was increased. Like Clifford, they also discovered instances of reduced heat transfer when compared with the stationary tube condition. They also found rotational buoyancy tended to suppress heat transfer with radially outward flow. With respect to stationary experiments they found no areas of impaired heat transfer.

The findings of Kheshi and Scriven [Ref 15] and Harasgama and Morris [Ref 16] were consistent. They found that as the Rossby number (which is the ratio of the mean through-flow velocity of fluid along the duct to a peripheral velocity formed by the product of the angular velocity and the hydraulic diameter ($\Omega d/V$)) increased, the axial velocity on one side decreased with respect to the other side and a cross

channel flowfield developed which was perpendicular to the main flow. The steady state for this condition showed that a two-vortex pattern developed. Increasing the Rossby number further generated a four-vortex flow pattern in the steady state. This four-vortex pattern required a shear-free flow to develop on both the top and bottom walls. The experiment suggested the flow pattern was a function of the aspect ratio of the channel, the Rossby number and the Ekman number. The Ekman number is defined as the ratio of the Rossby number to the Reynolds number [Ref 17]. Harasgama and Morris confirmed the effect of heat transfer on both the leading and trailing edges with either outward or inward flow. In addition they put a value of 10-20% on the decrease of the heat transfer on the leading side during outward flow. They attributed the increase in trailing side heat transfer to the strengthening of secondary flow as the average Nusselt number increased.

Hajek et. al. [Ref 18] investigated the impact of the rate of rotation and the difference in the temperature between the coolant and the wall (ΔT). By increasing ΔT the heat transfer either remained constant or increased. This increase was greater for walls with turbulators, although the percentage was not. This was a result of the higher heat transfer to walls with turbulators. When these increases, which could be larger, were compared to their larger initial values, smaller percentage increased were found. Increasing the Rossby number induced higher heat transfer on the trailing surface while at

the same time decreasing the leading surface value. They also developed the buoyant parameter (BP) such:

$$BP=\left(\frac{\Delta p}{\rho}\right)\left(\frac{\Omega D_h}{V}\right)\left(\frac{\Omega W}{V}\right) \quad (3)$$

where Δp is the pressure differential, ρ is the density of the coolant, Ω is the angular velocity, W is the eccentricity of the mid cross-sectional plane of the duct, V is the mean coolant velocity along the duct and D_h is the hydraulic diameter of the duct. By increasing this value, a higher heat transfer occurred on the trailing surface, while the leading surface initially experienced a decrease with a subsequent increase when BP approached the 0.2 to 0.4 range. In general they found that the locus of maximum heat transfer ratios for each Rossby number was a function of BP.

Taslim, Rahman and Spring [Ref 19] also confirmed that an increase of heat transfer occurred for both the rotating and stationary cases in a single pass channel when staggered rows of turbulators were added on opposite walls. The main thrust of this experiment was to explore the effect of Coriolis forces on internal heat transfer. In addition, they investigated the effect of varying the blockage ratio, e/D_h, where e denotes the turbulator height and D_h designates the hydraulic diameter of the passage. Their experiments found a blockage ratio of 0.1333 produced a maximum heat transfer coefficient increase of 45% and a ratio of .333 generated a minimum, a 6% decrease. Guidez [Ref 20] used a rotating

channel to correlate Reynolds number and Nusselt number to heat transfer coefficient. His results indicated that the pressure (or trailing) side of the channel experienced slightly increased, heat transfer as the Reynolds number increased while the suction side heat transfer was weaker. He determined the turbulence at the higher Reynolds number became larger than the turbulence induced by the rotation. His ratio of rotating Nusselt number to the stationary Nusselt number increased from 1.0 to 1.75 as the channel accelerated from 0 to 600 radians/sec on the pressure side. The ratio on the suction side decreased from 1.0 to 0.7 and reached a steady state value at approximately 175 radians/sec.

Wagner et. al. [Ref 21] performed an in-depth experiment to determine the effects that forced convection, Coriolis, buoyancy and flow direction had on heat transfer. For outward flow, changes in density ratio and Rossby number significantly affected the heat transfer. Altering the buoyancy parameter for this flow caused large changes in the heat transfer for the high pressure side, while changes made during inward flow produced minimal changes in the heat transfer. Density ratio and Rossby number also contributed minimally during inward flow. The suction side of the channel proved relatively immune to changes in heat transfer caused by modifying the density ratio, Rossby number or the flow direction. The heat transfer was more a function of the buoyancy than any other parameter.

Morris and Hanami-Nasr [Ref 22] found similar results in the actions of outwardly directed flow. They found enhanced heat transfer on the pressure wall resulted from Coriolis induced secondary flow and a reduction on the suction face. They determined that turbine blades designed from heat transfer measurements made on stationary models could experience failures attributable to the inability to predict local hot spots.

Investigating the effects of channel and turbulator geometry on internal heat transfer, Taslim et. al. [Ref 23 and 24] investigated a spanwise rotating channel. In both of these experiments, two walls of a channel contained turbulators arranged at an angle of attack to the direction of flow (α) of 45° in a criss-cross arrangement. In both experiments, blockage ratios, aspect ratios and Reynolds numbers were varied in an attempt to determine their effect on heat transfer coefficients. Using the Rotation number, which is defined as;

$$Ro = \frac{\Omega D_h}{U_m} = \frac{1}{Rossby\ Number} \qquad (4)$$

where Ω is the angular velocity, D_h is the hydraulic diameter and U_m denotes the mean velocity of air, the results of both investigations showed rotational effects to be more pronounced when the test sections possessed higher aspect and lower blockage ratios. Specifically, a steady increase in heat

transfer coefficient observed on the trailing side as the Rotation number increased while the heat transfer coefficient on the leading side showed a steady decrease.

C. COMPUTATIONAL INVESTIGATIONS

Taylor et. al. [Ref 25], Moore and Moore [Ref 26], Medwell et. al. [Ref 27], Patankar and Prakash [Ref 28], Rowley and Patankar [Ref 29] and Patankar and Kelkar [Ref 30] all reported results relevant to the next phase of the present investigation: a computational fluid dynamic analysis of cooling airflow inside a turbine blade. All used a finite volume analysis which produced good correlation to either problems they ran concurrently or to rudimentary experiments performed previously. In addition, by including the conduction in the solid boundary and avoiding upwind techniques, they concluded that this procedure will prove to be exceedingly successful with more complex shapes in the future.

D. PURPOSE

Numerous experiments have been performed to investigate the flowfield associated with an internally cooled turbine blade. There have been considerably fewer attempts to analyze this flow using numerical techniques. The purpose of the present analysis is to use Phoenics, a PC-based computational fluid dynamics program, to assist in predicting and

understanding the flowfield based upon the experimentations of Taslim and Spring [Ref 7].

II. THEORY

A. GOVERNING EQUATIONS

For a Newtonian fluid with no body forces, the law of Conservation of Mass becomes the continuity equation, Newton's Second Law yields the momentum equation and the First Law of Thermodynamics produces the energy equation. To correctly and fully describe fluid flow it is often necessary to include additional equations designed to model turbulence in the analysis. Finally additional equations are necessary to characterize the relationship between various fluid properties. An example of such an equation is the equation of state.

1. The Continuity Equation

When considering fluid flow through a fixed control volume, the continuity equation is:

$$\frac{\partial \rho}{\partial t} + \nabla \cdot (\rho \vec{V}) = 0 \qquad (5)$$

where ρ is the fluid density and V with the overhead arrow is the total velocity vector and u and v are velocity components in the x and y directions for two dimensional flow. Using the substantial derivative

$$\frac{D()}{Dt} \equiv \frac{\partial()}{\partial t} + \vec{V}\cdot\vec{\nabla}() \tag{6}$$

equation 5 becomes

$$\frac{D\rho}{Dt} + \rho\,(\vec{\nabla}\cdot\vec{V}) = 0 \tag{7}$$

For incompressible flow

$$\frac{D\rho}{Dt} = 0 \tag{8}$$

and equation 7 for incompressible two-dimensional flow becomes

$$\vec{\nabla}\cdot\vec{V} = \frac{\partial u}{\partial x} + \frac{\partial v}{\partial y} = 0 \tag{9}$$

2. The Momentum Equation

The momentum equation for two-dimensional flow and in conservative form is [Ref 31]

$$\frac{\partial \rho u}{\partial t} + \frac{\partial \rho u^2}{\partial x} + \frac{\partial \rho uv}{\partial y} + \frac{\partial p}{\partial x} - \frac{\partial \tau_{xx}}{\partial x} - \frac{\partial \tau_{xy}}{\partial y} = 0 \tag{10}$$

$$\frac{\partial \rho v}{\partial t} + \frac{\partial \rho uv}{\partial x} + \frac{\partial \rho v^2}{\partial y} + \frac{\partial p}{\partial y} - \frac{\partial \tau_{xy}}{\partial x} - \frac{\partial \tau_{yy}}{\partial y} = 0 \tag{11}$$

Here the viscous effects of the flow are described using the shear stress terms τ_{xx}, τ_{xy} and τ_{yy} where

$$\tau_{xx}=\frac{2}{3}\mu\left(2\frac{\partial u}{\partial x}-\frac{\partial v}{\partial y}\right) \quad (12)$$

$$\tau_{xy}=\mu\left(\frac{\partial u}{\partial y}+\frac{\partial v}{\partial x}\right) \quad (13)$$

$$\tau_{yy}=\frac{2}{3}\mu\left(2\frac{\partial v}{\partial y}-\frac{\partial u}{\partial x}\right) \quad (14)$$

Now introducing Reynolds averaging, equations 10 and 11 rewritten for incompressible flow assume the following forms

$$\frac{\partial\rho\overline{u}}{\partial t}+\frac{\partial\rho\overline{u}^2}{\partial x}+\frac{\partial\rho\overline{u}\,\overline{v}}{\partial y}=-\frac{\partial\overline{p}}{\partial x}+\frac{\partial}{\partial x}\left(\overline{\tau}_{xx}-\rho\overline{u'u'}\right)+\frac{\partial}{\partial y}\left(\overline{\tau}_{xy}-\rho\overline{u'v'}\right) \quad (15)$$

$$\frac{\partial\rho\overline{v}}{\partial t}+\frac{\partial\rho\overline{u}\,\overline{v}}{\partial x}+\frac{\partial\rho\overline{v}^2}{\partial y}=-\frac{\partial\overline{p}}{\partial y}+\frac{\partial}{\partial x}\left(\overline{\tau}_{xy}-\rho\overline{u'v'}\right)+\frac{\partial}{\partial y}\left(\overline{\tau}_{yy}-\rho\overline{v'v'}\right) \quad (16)$$

where the reduced forms

$$\overline{\tau}_{xx}=\mu\left(2\frac{\partial\overline{u}}{\partial x}\right) \quad (17)$$

$$\overline{\tau}_{xy}=\mu\left(\frac{\partial\overline{u}}{\partial y}+\frac{\partial\overline{v}}{\partial x}\right) \quad (18)$$

$$\overline{\tau}_{yy}=\mu\left(2\frac{\partial\overline{v}}{\partial y}\right) \quad (19)$$

apply. In equations 10 through 19, u and v are the velocity components in the x and y direction respectively , ρ is the fluid density, p is the fluid pressure and μ is the fluid viscosity. All terms with an over bar indicate a time averaged quantity, while terms with a primed superscript indicate fluctuation quantities.

3. The Energy Equation

Applying the First Law of Thermodynamics to a fluid passing through a control volume yields

$$\rho C_p \frac{DT}{Dt} = \frac{Dp}{Dt} + \nabla(k\nabla T) + \Phi \qquad (20)$$

where the total energy is comprised only of internal and kinetic energy. The form of equation 20 for heat transfer in incompressible two-dimensional flows is written in terms of static temperature as

$$\rho C_p \frac{\partial \overline{T}}{\partial t} + \rho C_p \frac{\partial}{\partial x}(\overline{u}\ \overline{T}) + \rho C_p \frac{\partial}{\partial y}(\overline{v}\ \overline{T}) =$$
$$\frac{\partial \overline{p}}{\partial t} + \overline{u}\frac{\partial \overline{p}}{\partial x} + \overline{v}\frac{\partial \overline{p}}{\partial y} + \overline{u'\frac{\partial p'}{\partial x}} + \overline{v'\frac{\partial p'}{\partial y}} + \qquad (21)$$
$$\frac{\partial}{\partial x}\left(k\frac{\partial \overline{T}}{\partial x} - \rho C_p \overline{u'T'}\right) + \frac{\partial}{\partial y}\left(k\frac{\partial \overline{T}}{\partial y} - \rho C_p \overline{v'T'}\right) + \overline{\Phi}$$

where the dissipation function, Φ overbar, is

$$\overline{\Phi} = \overline{\tau_{xx}}\left(\frac{\partial \overline{u}}{\partial x}\right) + \overline{\tau_{xy}}\left(\frac{\partial \overline{u}}{\partial y} + \frac{\partial \overline{v}}{\partial x}\right) + \overline{\tau_{yy}}\left(\frac{\partial \overline{v}}{\partial y}\right) \qquad (22)$$

and the fluctuating dissipation function has been ignored. [Ref 32]

4. Turbulence Modeling

The unsteady Navier-Stokes equations are believed to describe turbulent fluid flow. Currently the primary technique employed in computational fluid dynamic predictions of fluid flow and heat transfer is to use the time-averaged Navier-Stokes equations. These take the randomly generated

flow variables and decompose them into their time averages and their instantaneous fluctuations. The time averages in this report are indicated with the overbar symbol while the fluctuations are given the apostrophe superscript. These new terms are interpreted as apparent stress gradients and heat-flux quantities associated with turbulent motion. These quantities can then be related to the mean flow variables through turbulence models.

For the present analysis, the turbulence model used is the two equation model, commonly referred to as the k-ε model, discussed by Launder and Spalding [Ref 33]. The value for the effective turbulent viscosity, μ_T, is

$$\mu_T = \rho C_\mu \frac{k^2}{\varepsilon} \tag{23}$$

where C_μ equals 0.09, k is the kinetic energy of turbulence and ε is the turbulence dissipation rate. They derived two transport equations to define their turbulence model. The turbulence kinetic energy transport equation is commonly modeled as

$$\rho \frac{\partial k}{\partial t} + \rho \vec{V} \cdot \nabla k = \nabla \left(\frac{\mu_T}{Pr_k} \nabla k \right) + \mu_t \Phi - \varepsilon \tag{24}$$

where Pr_k is the Prandtl number for the turbulent kinetic energy and is assumed to be 1.0. The other transport equation necessary to complete this turbulence characterization is the

one for the turbulence dissipation rate. This purely empirical formula is given as:

$$\rho \frac{\partial \varepsilon}{\partial t} + \rho \vec{V} \cdot \nabla \varepsilon = \nabla \cdot \left(\frac{\mu_T}{Pr_\varepsilon} \nabla \varepsilon \right) + C_{\varepsilon_2} \mu_T \frac{\varepsilon}{k} \overline{\Phi} - C_{\varepsilon_2} \rho \frac{\varepsilon^2}{k} \qquad (25)$$

In both of these equations several similarities appear. The left side of both equations equate to the particle rate of increase of the variable. The first term on the right side is the diffusion rate while the second and third terms are the production and dissipation, respectively.

This turbulence model proves more successful in the outer regions of the flow field as opposed to the inner region where convective transport is relatively unimportant. For this region wall functions have been developed for the area in the range of $30 < y^+ < 200$ where y^+ is defined as

$$y^+ = \frac{y(|\tau_w|/\rho_w)^{\frac{1}{2}}}{\nu_w} \qquad (26)$$

with τ_w being the shear stress, ρ_w the density and ν_w representing the kinematic viscosity all evaluated at the wall. Employing these wall functions in the near wall region eliminates the need for a much finer grid in this area.

B. THE GENERAL DIFFERENTIAL EQUATION

Patankar [Ref 34] and Patankar and Spalding [Ref 35] recognized the relationship of the terms in the model transport equations and advocated a procedure of numerical

analysis of fluid flow which involves a general differential equation. Their equation is

$$\frac{\partial}{\partial t}(\rho\phi) + \nabla\cdot(\rho\vec{u}\phi) = \nabla\cdot(\Gamma\nabla\phi) + S \qquad (27)$$

where ϕ represents the dependent variable and Γ and S refer to the diffusion coefficient and the source term, respectively. These quantities are distinctive for the ϕ being analyzed.

The realization that the applicable transport equations of momentum, the energy, turbulence kinetic energy and dissipation and related coefficients can be thought of as particular cases of the general ϕ equation is an important time-saving step. Now for the solution of a fluid flow and heat transfer problem, only the numerical solution of equation 27 need be investigated. By constructing the applicable computer algorithm based on a pressure correction scheme [Ref 34] in such a manner as to repeatedly solve this same equation with an appropriate definition for ϕ and the pertinent values of Γ and S, considerable computational time and memory savings are realized.

C. BOUNDARY CONDITIONS

1. Boundary Conditions at a Wall

No-slip boundary conditions are used for the velocities at a solid wall, where they are all set equal to zero. Wall temperatures are either explicitly set or the temperature gradient at them is specified. When the flux at

the wall is set equal to zero the wall assumes the properties of an adiabatic wall.

2. Boundary Conditions at Inflow

The conditions at the inflow include all the velocity, pressure, temperature and turbulence intensity. For this investigation these values were all specified at the inlet condition.

3. Boundary Conditions at Outflow

The outflow of this problem required only the specification of the pressure to atmospheric conditions. All other conditions at the outflow were extrapolated by the analysis.

III. THE PHOENICS COMPUTATIONAL PROGRAM

A. HOW THE PHOENICS COMPUTATIONAL PROGRAM WORKS

Phoenics is a computer code which simulates fluid-flow, heat-transfer,chemical-reaction and related phenomena. It is capable of solving three-dimensional, unsteady and turbulent flow problems. Relying on the validity of the assumptions used to generate the input, it has the ability to simulate the effects of interaction between such phenomena and the surrounding environment. Phoenics was used throughout this investigation. For each dependent variable ϕ, Phoenics generates as many difference equations as cells within the domain. Thus, the total number of equations Phoenics must solve is x times y times the number of dependent variables present in the domain. Not only are these equations numerous, but they are also very strongly coupled. In addition they are also characteristically non-linear due to the functional dependence of the coefficients and sources upon the auxiliary and dependent variables. To solve these non-linear equations, Phoenics employs an iterative predict-and-correct technique which reduces the imbalance between the left and right sides of each equation to a negligible level.

B. GRID GENERATION

Phoenics can implement and use Cartesian, cylindrical polar or curvilinear or body-fitted coordinates. For two-dimensional Cartesian grids, specification of the length and height of the area of analysis is required. The area between the x and y boundaries can then be filled with as many grid lines as the solution requires. Spacing of these lines is either uniform, exponential (with continually increasing or decreasing spacing), or in a "power" arrangement, which both increases and then decreases the spacing of the grid lines. These last two options allow the generation of a grid permitting clustering of the grid points closer together near the boundaries. When different regions are designated, the spacing can vary from region to region as necessary. In addition, by stipulating various regions in the x or y direction, irregular shapes can be analyzed by placement of zero-porosity obstructions which eliminate the zones from the flow field.

IV. BACKGROUND ON THE TURBULATOR DUCT PROBLEM

A. EXPERIENCE ON CASTING PROBLEMS IN TURBINE BLADES

As shown in Chapter I, internally routed cooling air flow proves quite effective in permitting higher internal operating temperatures for gas turbine engines particularly if turbulators are used in the coolant passages. The size, shape and orientation of the duct and the geometry of the turbulators within these ducts is crucial to the convective removal of heat from the blades. As many investigations showed, altering the aspect ratio of the duct or the turbulators, the spacing of the turbulators, their orientation, the turbulator pitch-to-height ratio and their shape, greatly impacts their effectiveness in promoting heat transfer.

With the continual emphasis on reduction of weight for today's aircraft and their components, engine dimensions, both externally and internally, are also decreasing. For this reason the casting process by which turbine blades are manufactured is placing restrictions on the size and shape of the turbulators which can be employed. During the turbine blade casting process one of the problems encountered involves the inability of the molten materials to totally fill the grooves forming the turbulator.

A second problem is the tolerances provided by the manufacturing process. Current turbine sizes require turbulators measuring approximately 0.010" in height. The lower limit for associated dimensional tolerances is 0.002" - 0.003". Thus a turbulator designed for a height of 0.010" can have a variance of up to 30%. This difference can significantly effect the heat transfer coefficient for an engine where a 0.010" turbulator presents a high blockage ratio.

B. AN EXPERIMENTAL INVESTIGATION INTO A TURBULATED DUCT

1. Background and Duct Construction

Taslim and Spring [Ref 7] performed a series of experiments to determine the variation in heat transfer caused by the geometrical changes characteristic of small cast airfoils. Their method involved using a 46 inch long channel constructed of plexiglas on three sides, with the fourth side made of a polyurethane slab incorporating a series of heaters and liquid crystal sheets. The width of the heated wall was 3", which fixed that dimension for the duct. The length of the side walls were changed to alter the aspect ratio during the experiment. Experiments were run with aspect ratios for the duct alternating between 0.50 and 0.55.

The first 14 inches of the duct had no turbulators and simulated the unturbulated area at the root of the airfoil, while the final 32 inches contained a staggered array of

turbulators on the heated face and the opposing plexiglass wall. During the experiment, turbulator height, e, center-to-center pitch, S, and turbulator width, w, were varied. Blockage ratios, e/D_h where D_h is the hydraulic diameter, ran between 0.15 and 0.285, while pitch-to-height ratios, S/e, varied between 4.27 and 14.2.

2. Conduct of the Experiment

After calibrating the liquid crystal sheets in a water bath so a given temperature produced a known color, and with the desired turbulator and duct configuration established, air flow was introduced into the duct with a set mass flow rate. This combination of duct geometry and mass flow rate established the Reynolds number for the test run.

Selecting an area approximated by $x/D_h = 16$, where x is the distance from the test section entrance and D_h is the hydraulic diameter of the unturbulated section, the heat flux was varied by increasing or decreasing the power on the wall heaters until a reference color was obtained on the downstream side of a turbulator near the selected area. A picture of this area was taken and the power altered until the same reference color was achieved in the next adjacent area. This process was repeated until the entire area between the pair of turbulators was covered.

The final experimental step required digitizing each picture and measuring the area covered by the reference color.

This allowed production of an area-weighted average heat transfer coefficient.

3. Results

The first result desired from the experiment was to determine the impact of alleviating the problems caused by the aforementioned non-fill difficulty by reducing the aspect ratio of the turbulator, AR_t. Taslim and Spring [Ref 7] found a reduction of AR_t from two to one reduced the Nusselt number on the turbulated wall by 33% for high blockage ratio turbulators (e/D_h =0.22) with a spacing of S/e of 5. As expected, a reattachment point formed directly downstream of the turbulators. This was the point of maximum heat transfer coefficient, which then decreased monotonically in the downstream direction until it approached the next turbulator, where it started to increase again. The conclusion from this analysis was that an optimum spacing between turbulators existed which allowed sufficient length for the flow to reattach, and then a minimum of spacing thereafter to the next turbulator. The conclusion was that, for a square turbulator (AR_t = 1) with a relatively high blockage ratio, the optimum S/e spacing was approximately 8.5.

After this determination, the effects of rounding the turbulators at the tops and decreasing the sharpness of the fillets were investigated. Testing was performed on four sets of turbulators. Two sets were manufactured, both with an AR_t

of 1.0, with one set having sharp fillets and sharp corners and the other having rounded fillets and rounded corners. Two similar sets were constructed with an AR_t of 2.0, with the sharp or rounded fillets and corners. As expected the rounding decreased the Nusselt numbers on the turbulated walls for both AR_t's, but the AR_t = 2.0 configuration produced a 17% reduction over the sharp cornered turbulators with the same AR_t, while the difference for the turbulators with an AR_t of 1.0 was only 5%. Concurrently incorporated was a reduction of 8.6% of surface area for the turbulator with an AR_t of 2 and a 7.15% reduction for the other set. The contrast was attributed to the difference in spacing between the sidewalls of the adjacent turbulators. Although the S/e was held constant, the lower AR_t turbulators were wider and hence less distance existed between sidewalls. Thus for higher aspect ratio turbulators, the flow had sufficient length to reattach after the turbulator, while for the lower aspect ratio, reattachment did not occur. In the latter case (tip-to-tip turbulator flow) there was less dependence on turbulator geometry.

From these results an optimum turbulator design could be attempted. For manufacturability, the corners would be rounded and the base would be wider. For maximum heat transfer the tip would be kept narrow. The resulting rounded trapezoidal shape is termed a "jersey-barrier". At S/e of

five the jersey-barrier shaped turbulators exhibited the same Nusselt number as high AR_t turbulators.

Another area investigated was the impact of manufacturing tolerances on the heat transfer characteristics of turbulated ducts. Using a jersey-barrier shaped turbulator with a nominal height of 0.010" and a tolerance of ± 0.003" on S/e of 10, a ±40% deviation in the turbulated wall Nusselt number was experienced when dimensions were allowed to approach their minimum and maximum tolerance values. Reducing the S/e ratio to 5, caused a variation from the nominal case of +22% and -13% from the maximum to minimum profiles.

The final area examined was the interaction between the blockage ratio, the pitch-to-height ratio and the turbulator aspect ratio. It was found that the decrease in Nusselt number associated with a reduction in e/D_h could be completely offset by increasing the AR_t and S/e. In addition, with a constant S/e close to the optimum level and a moderate blockage ratio, decreasing the AR_t from 1.0 to 0.625 resulted in only a 7% drop in the Nusselt number. This was characteristic for geometries with the S/e closer to the optimum value (8.5) and a lower value for the blockage ratio.

V. PHOENICS SIMULATION OF THE TURBULATOR DUCT EXPERIMENT

The Phoenics program was used to compute the results of the previous turbulated duct experiment. The analysis was divided into two basic steps. The first was to generate a rectangular straight duct with one wall heated. By controlling the Reynolds number, through varying inflow velocity, the Dittus-Boelter correlation of $NU_s=.0243Re^{0.8}Pr^{0.4}$ was verified [Ref 31]. The simulation was two-dimensional.

The second phase was the generation of a turbulated duct to reproduce experimentally obtained results through numerical analysis. Again a rectangular two-dimensional straight duct was used with a staggered arrangement of turbulators on the top and bottom wall. The bottom wall was heated.

A. DUCT AND FLOWFIELD SETUP

1. Grid Generation

a. Unturbulated Square Duct

The first duct to be modeled was 30.0m long. The height of the duct was 1.0m and it contained no turbulators. The bottom wall was heated.

In the x direction the entire duct was considered one region. It was divided into 100 grid points which were stretched in the x direction using a factor of 1.10. This configuration clustered the grids near the inlet. By doing

so, the grid cells were square at the entrance to the region, which insured that the flow achieved its fully developed profile prior to entering the zone where it was analyzed.

In the y direction there was only one region. There were 50 grid points along the y axis and they were clustered along the top and bottom walls.

b. Turbulated Rectangular Duct

In the second phase two ducts were generated. The first duct was 1.17m long with the initial 0.356m unturbulated. The turbulators had an aspect ratio, AR_t, of 1.0, with a height, e, of 0.0127m and a turbulator center-to-center pitch, S, of 0.0635m. All the turbulators were square, with sharp corners and fillets. The first turbulator was on the top wall and all were positioned 90° to the flow. The second duct was 0.654m long, with the same unturbulated region at the inlet. The duct aspect ratio remained the same. Ten turbulators of the same AR_t, S, and e were again positioned 90° to the flow, with the first one on the top wall. The bottom wall of both ducts in the second phase was heated.

The longer duct was divided into 30 regions along the x axis. It included 175 grid points which were stretched by a factor of 1.2. Region two and every fourth region thereafter(6,10,14,...) through number 26 were the regions designated for the turbulators on the top wall. Similarly region four and every fourth region following through number 28 were

the regions demarcating the locations of the bottom turbulators. All of the regions designating the turbulators were 0.0127m long and contained seven grid points. The odd numbered regions through number 29 specified the spaces between the upper and lower turbulators. Each was composed of nine grid points and was 0.0191m in length. The final region was 0.369m long and modeled outflow from the duct. No turbulators were located here and it contained 101 grid points.

In the vertical direction three regions were specified. The first region was from the bottom wall up 0.0127m, which corresponded to the height of the turbulators. It contained 15 grid points. The second region extended from the top of the first up 0.0165m. Twenty-five grid points were allocated in this region. The final region in the y direction simulated the top wall turbulators. Like region one it was 0.0127m tall and held 15 grid points. Figure 1 shows a schematic of the longer duct with an enlarged segment which depicts the grid at the end of the first region and the first two turbulators in the turbulated region.

This grid most closely resembled the experiment, but did not give adequate grid resolution. An additional duct was generated, which had a finer mesh size. This duct was a shortened version of the fully turbulated one. As will be explained, investigation revealed that the shorter length did

not significantly alter the flowfield prediction and did allow a greater concentration of grid points throughout the duct. This final duct also included an unturbulated inlet region, whose dimensions and grid points were the same as the previous duct. The shortened turbulated region measured 0.298m long and consisted of ten turbulators arranged in a staggered array again with the first one on the top wall. Each turbulator has fifteen grid points from front to back and there are 20 grid points in the space between each turbulator. This duct was investigated using a uniformly spaced grid and stretching factors of 1.05, 1.10 and 1.20 all of which clustered the grids near the front and back of the turbulators. There were 325 grid points in this region and a total of 500 in the entire horizontal or streamwise direction.

The vertical direction was constructed the same way as the previous duct with three regions of fifteen, twenty-five and fifteen grids each. Grid spacing here also employed both stretched and uniformly spaced points. Figure 2 shows the same area for this duct as in Figure 1. Figure 2 uses the 1.2 level of grid spacing on the increased level of grid points.

2. Boundary Conditions

Analyses were run at a number of different Reynolds numbers and turbulence levels. The Reynolds number is defined as

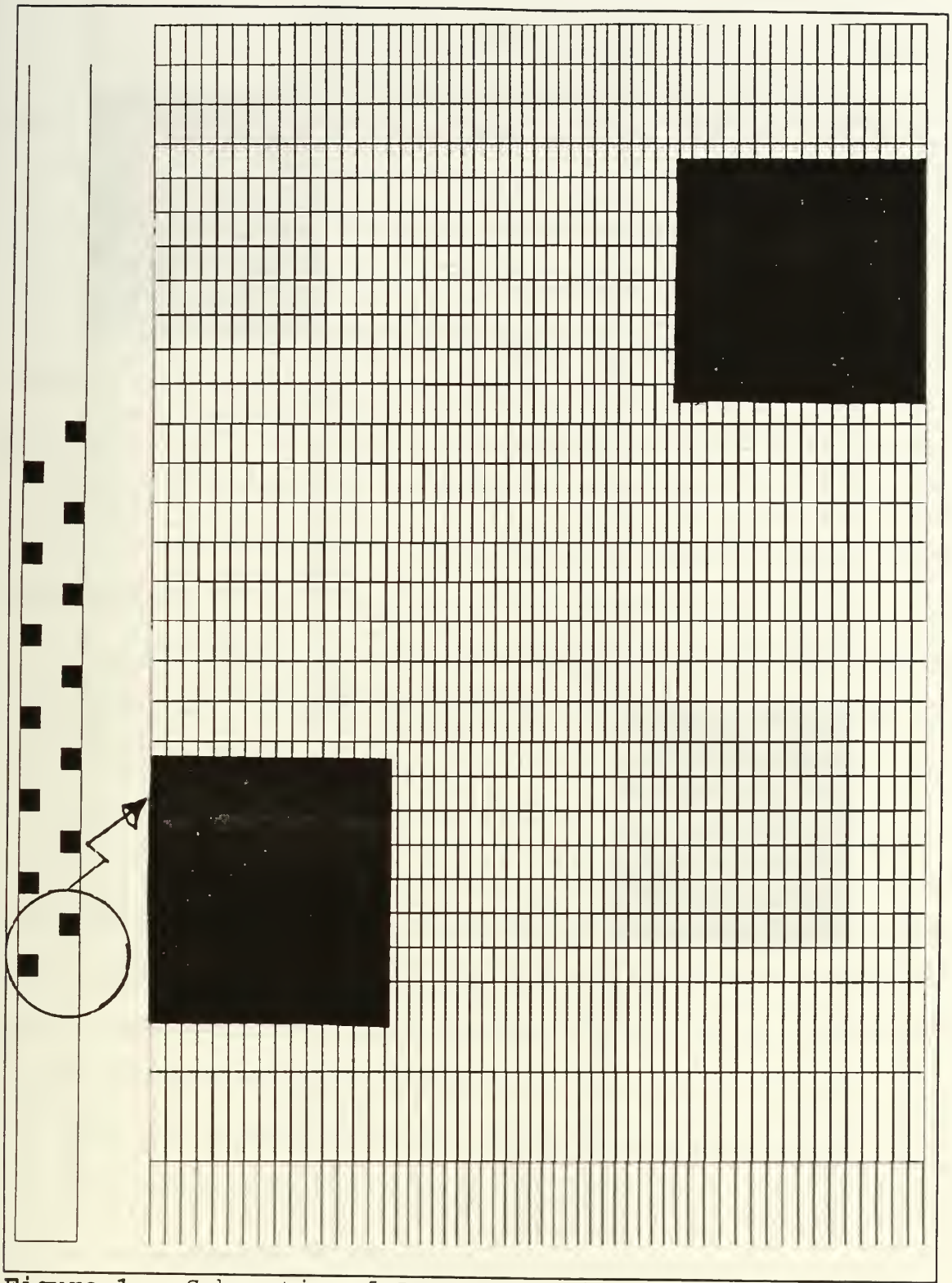

Figure 1 - Schematic of Long Duct With Enlargement of the First Two Turbulators Placed in a Uniformly Spaced Grid

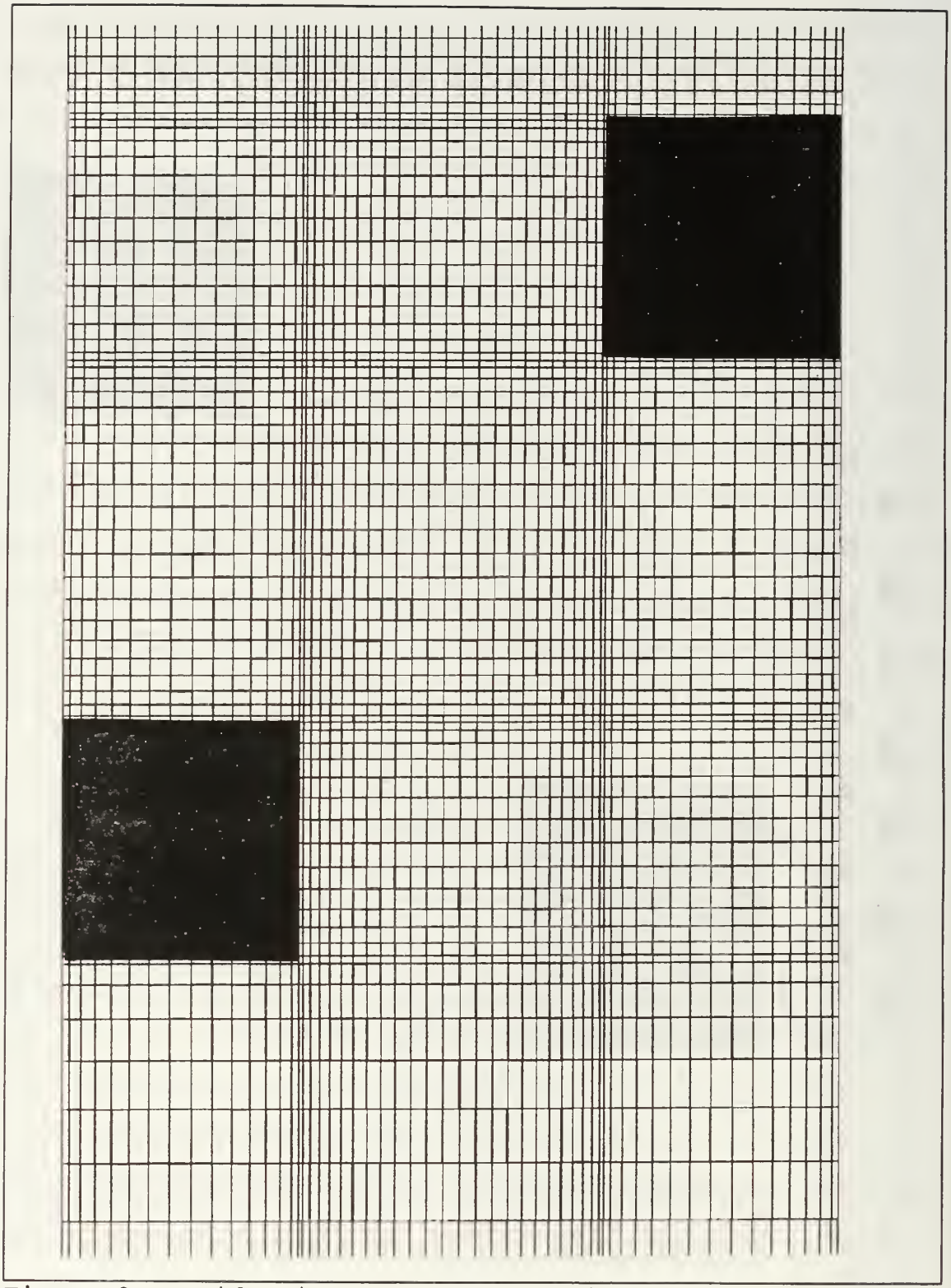

Figure 2 - Grid Using a 1.20 Stretching Factor

$$Re=\frac{\rho u D_h}{\mu} \tag{28}$$

where D_h is the hydraulic diameter. For a rectangular duct, D_h is defined as 4A/P where A is the area of the duct and P is the perimeter. For a two dimensional analysis a length scale is used. For the purposes of this investigation the D_h used was the value for the actual D_h of the duct as configured in Taslim's and Spring's experiment. Using the values for density of 1.161 kg/m^3 and for viscosity of 1.589 X 10^{-5} kg/m-s, Table 1 gives the inlet velocities in the horizontal direction associated with the Reynolds numbers which were investigated.

A value of 2% inlet turbulence was specified for a Reynolds number of 10000. The turbulent kinetic energy is calculated as follows

$$k=(\frac{1}{2}Tu)\times[u]^2 \tag{29}$$

where Tu is the turbulence intensity and u is the inlet velocity, the values for the appropriate turbulence levels to keep k approximately equal at the inlet for all Reynolds numbers is also given in Table 1.

REYNOLDS NUMBERS, VELOCITIES AND TURBULENCE LEVELS INVESTIGATED

Reynolds Number	Velocity (m/s)	Turbulence (%)
10000	2.531	2.000
15000	3.796	0.889
20000	5.062	0.500

Table 1

The inlet flow temperature was held at 300° K for all runs. The bottom wall was heated with a constant temperature of 400° K, and the top wall was specified as adiabatic. At the outlet the external static pressure was specified.

The turbulators were obstructions in the flow and so they were specified as non-conducting, adiabatic obstructions. In addition they were given the characteristics of possessing friction and having zero-porosity. No gravity forces, heat sources or internal plates were simulated in this analysis.

VI. COMPUTATIONAL RESULTS

A. UNTURBULATED PLANAR DUCT

As an initial test case an unturbulated square duct was evaluated by the Phoenics computational program. For fully developed laminar flow, a parabolic velocity profile develops with a maximum velocity, $u_{max}=2u_{mean}$. For turbulent flow the velocity profile is much flatter in the center due to the mixing motion and momentum exchange and $u_{max}\approx 1.2u_{mean}$.

The values of The Reynolds numbers for this investigation were 10000 and 20000. The geometry of the chosen duct provided a 30:1 length to height ratio. This allowed a sufficient length for the flow to develop fully prior to being investigated. The zone chosen for the analysis of the flow was located between 20 and 25 diameters downstream of the inlet.

Figure 3 is a profile of the flow located 25 diameters from the inlet. As can be seen it presents the classic shape associated with turbulent fluid flow in a duct. The maximum value of the velocity of the flow occurs at mid-duct and is a value of 0.1181 m/s. Using the Phoenics results file the mean average for velocity at this point in the flow was 0.998 m/s. The ratio is approximately 1.18, which is indicative of

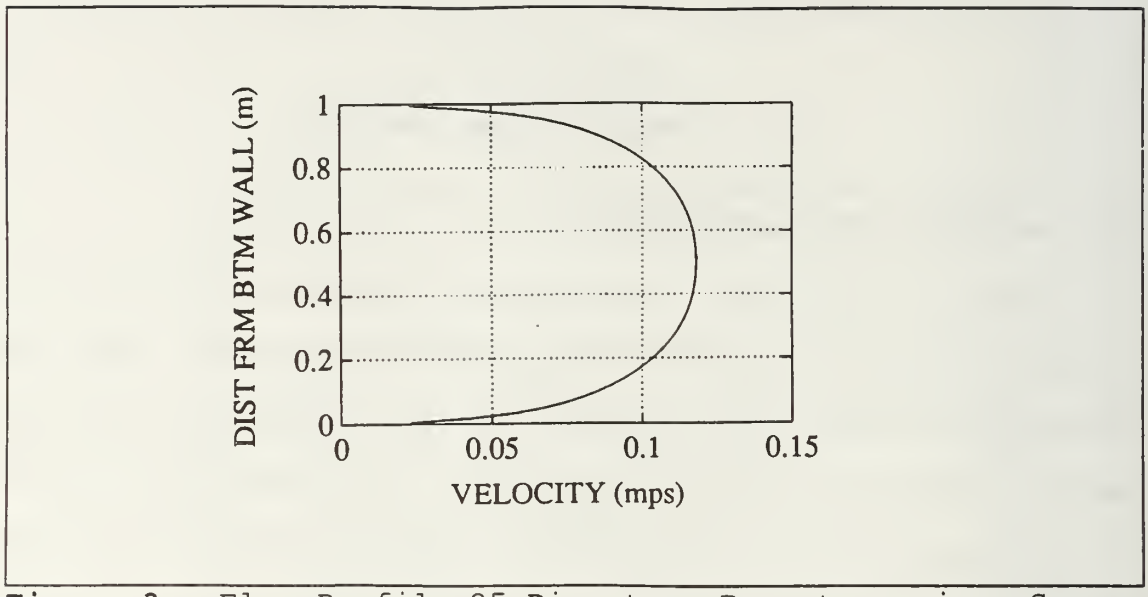

Figure 3 - Flow Profile 25 Diameters Downstream in a Square Unturbulated Duct

turbulent flow. A plot of the skin friction coefficient, c_f, where

$$c_f = \frac{\tau_w}{\frac{1}{2}\rho u^2 S} \qquad (30)$$

τ_w is the shear stress along the wall and S is the area, on the bottom wall (Figure 4) shows the increase associated with the viscous effects as the flow progresses along the duct. The value for this shear stress along the top and bottom wall for the area of fully developed flow is 8.175 X 10^{-5} kPa.

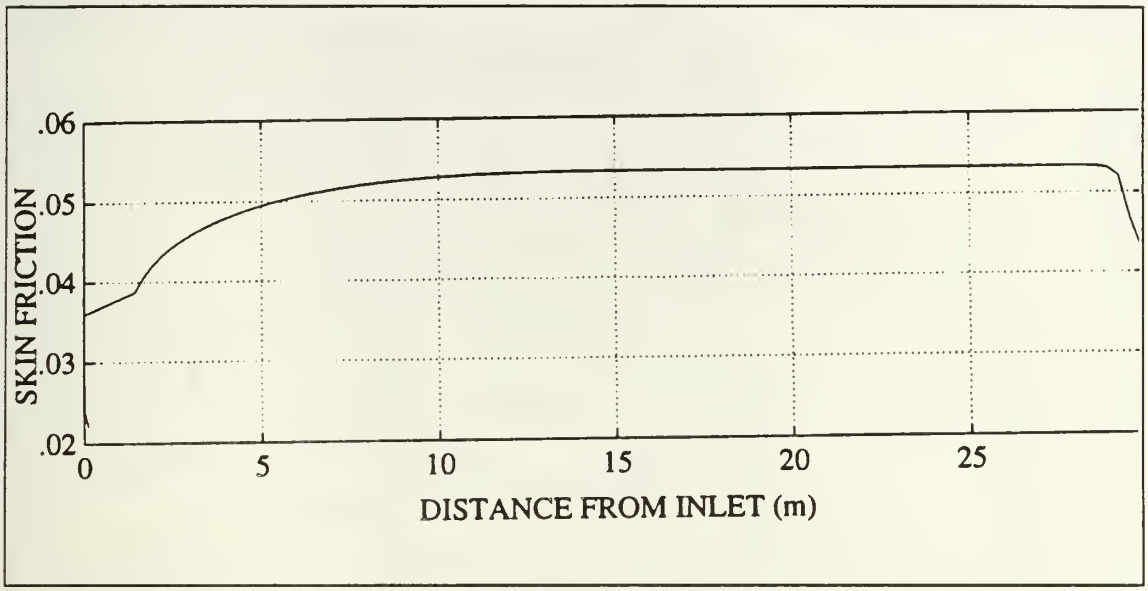

Figure 4 - Skin Friction Coefficient for the bottom Wall of a Square Duct

B. TURBULATED RECTANGULAR DUCT

1. Full Turbulated Duct

A solution for the turbulated full duct was generated first. As stated previously this analysis was run with a relatively coarse grid in order to simulate Taslim's [Ref 7] experiment. This run included a Reynolds number of 10000 and converged at approximately 1900 iterations.

As shown in Figure 5, at both the first and second turbulators the flow generated a stagnation point on the upstream face of the turbulator and recirculation occurred ahead of the turbulator. Figure 6 is a plot of the velocity vectors for the area of the duct adjacent to the second turbulator. The flow did not recirculate upstream of

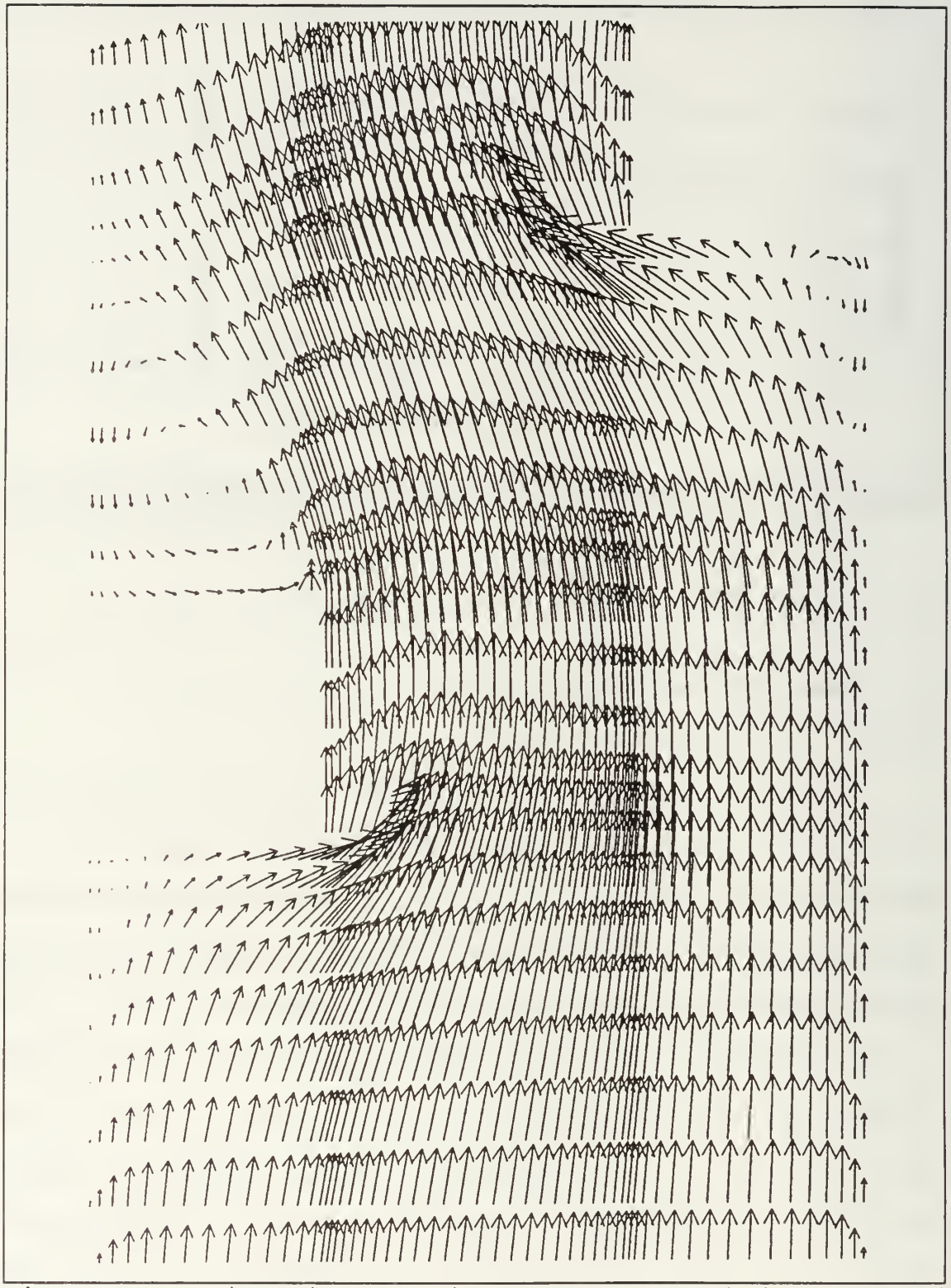

Figure 5 - x-Direction Velocity Vectors at Turbulators 1 and 2

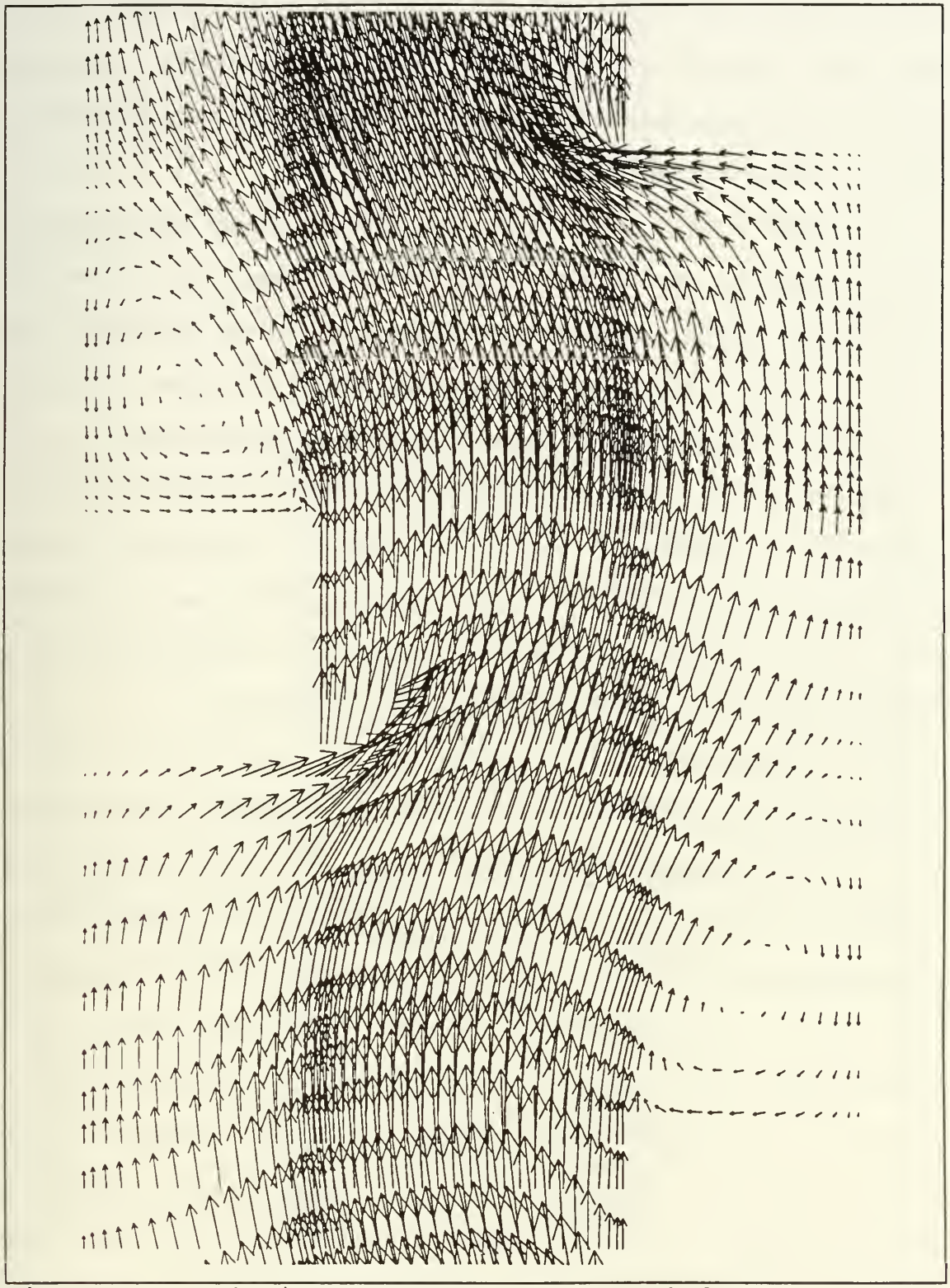

Figure 6 - Velocity Vectors Between Turbulators 2 and 4 Using a Constant Grid Spacing

turbulators three and four, because of the influence of the upstream turbulators two and three respectively. This flow pattern became repeatable from this location onward until the end of the turbulated section.

The position of the reattachment point downstream of the turbulator was dependent on the location within the duct. As the flow progressed down the duct, the reattachment point moved closer to the downstream face of the turbulator eventually reaching a fixed distance downstream of the turbulator. The area between turbulators eight and ten was the first to approximate this "periodic" flowfield. Figure 7 shows the vectors as they appeared for the flow in this area and Figure 8 plots the x-direction velocity components for the first grid point away from the lower surface.

Another area of interest was the behavior of the freestream kinetic energy (k) of the turbulence. The mid-duct value for turbulent kinetic energy was plotted for the entire length. Figure 9 shows an initial free stream decay of turbulence in the unturbulated section, after which the turbulence increased dramatically at the first turbulator and experienced additional increases at each subsequent one. Initially each gain was significant, but eventually they became smaller in magnitude. After the eighth turbulator a near constant value was approximated for the free-stream turbulence. This asymptotic value was two orders of magnitude over the minimum values experienced in the unturbulated

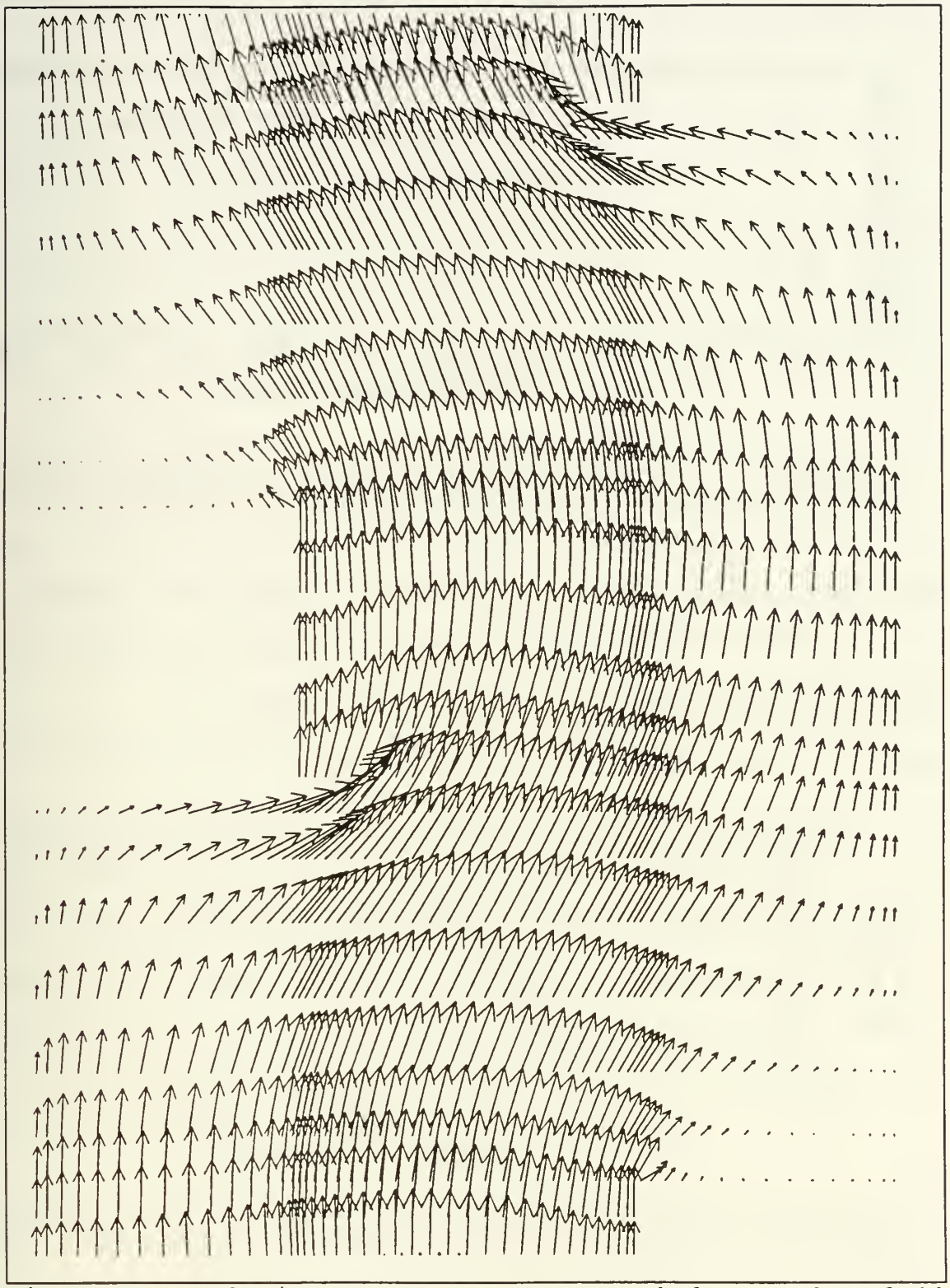

Figure 7 - Velocity Vectors Between Turbulators 8 and 10 Using a Constant Grid Spacing

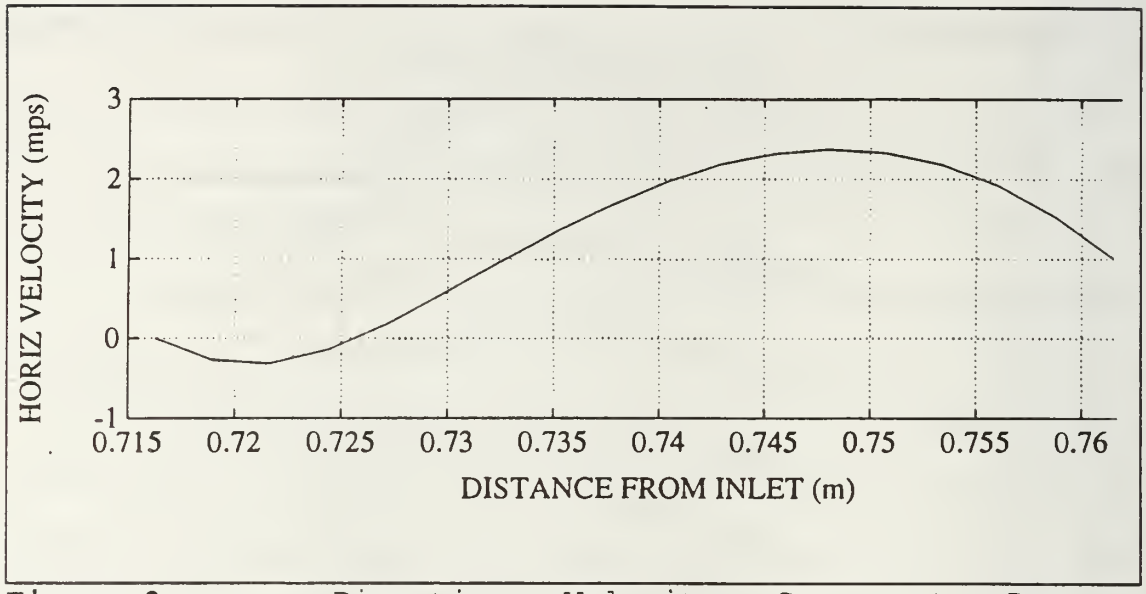

Figure 8 - x-Direction Velocity Component Between Turbulators 8 and 10 Using a Constant Grid Spacing

section. After the last turbulator, the flow entered the unturbulated outlet portion of the duct and turbulence once again decreased due to viscous dissipation.

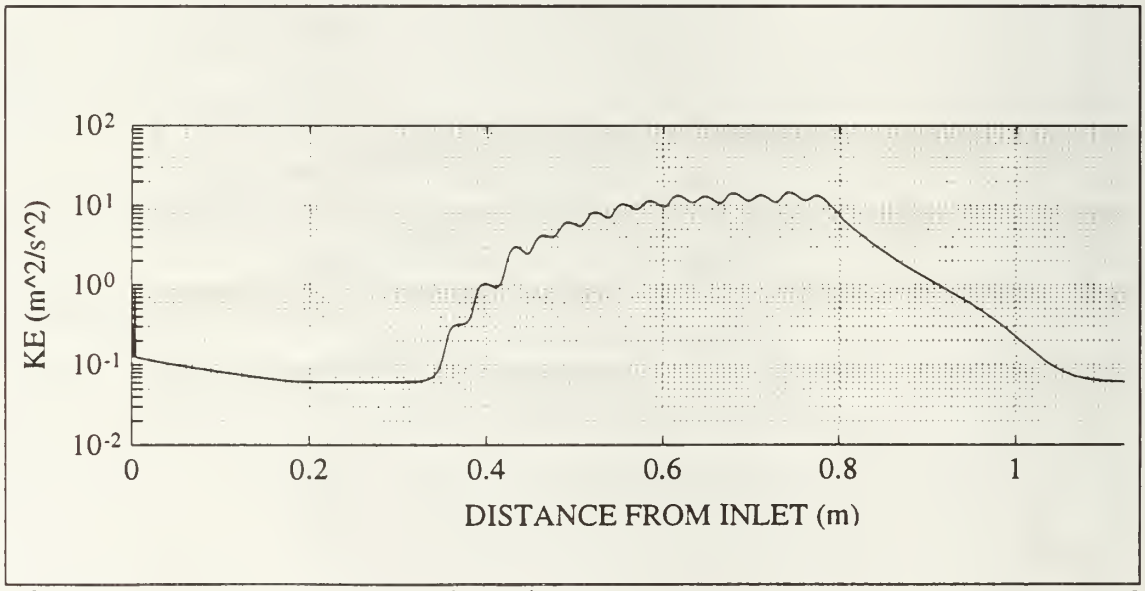

Figure 9 - Turbulent Kinetic Energy for a Full Turbulated Duct

Using the above data, the tenth turbulator was employed as the cutoff point for the full investigation.

2. Abbreviated Turbulated Duct

a. Uniformly Spaced Grid Simulation

Using a uniformly spaced grid and a duct shortened to ten turbulators, a simulation was run at a Reynolds number of 10000 with a turbulence intensity of 2.0%. The development of the flow was consistent with the full length duct. Both the first turbulator (on the top wall) and the second one (on the bottom wall) developed regions of recirculation prior to them. Figure 10 is a plot of the velocity vectors for the area prior to turbulator two and it shows the flow pattern with a distinct stagnation point.

The flow for the area downstream of turbulator two, however was markedly different from the structure found using the full length duct. Here the entire area between the second and fourth turbulators exhibited recirculation of the flow. No reattachment point along the bottom wall existed. Figure 11 is a plot of the vectors in this area and shows the total reverse flow. A plot of the horizontal velocity at the first grid line off the bottom wall for this region shows the negative value of this component in Figure 12.

After the fourth turbulator, the flow along the bottom wall begins to exhibit the characteristics of the previous duct. The flow over the turbulator turns down to the

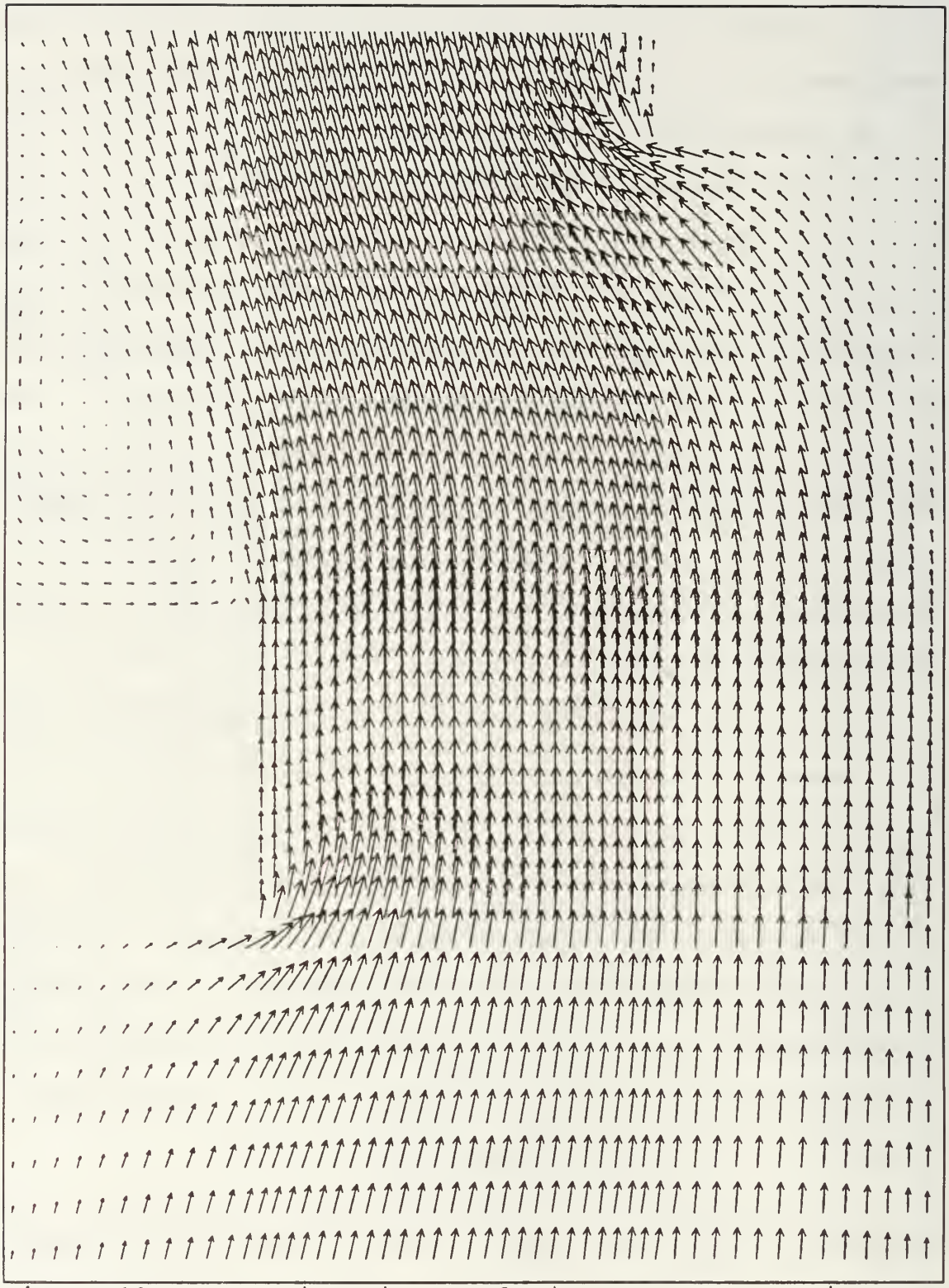

Figure 10 - x-Direction Velocity Vectors Prior to Turbulators 1 and 2 Using a Constant Grid Spacing

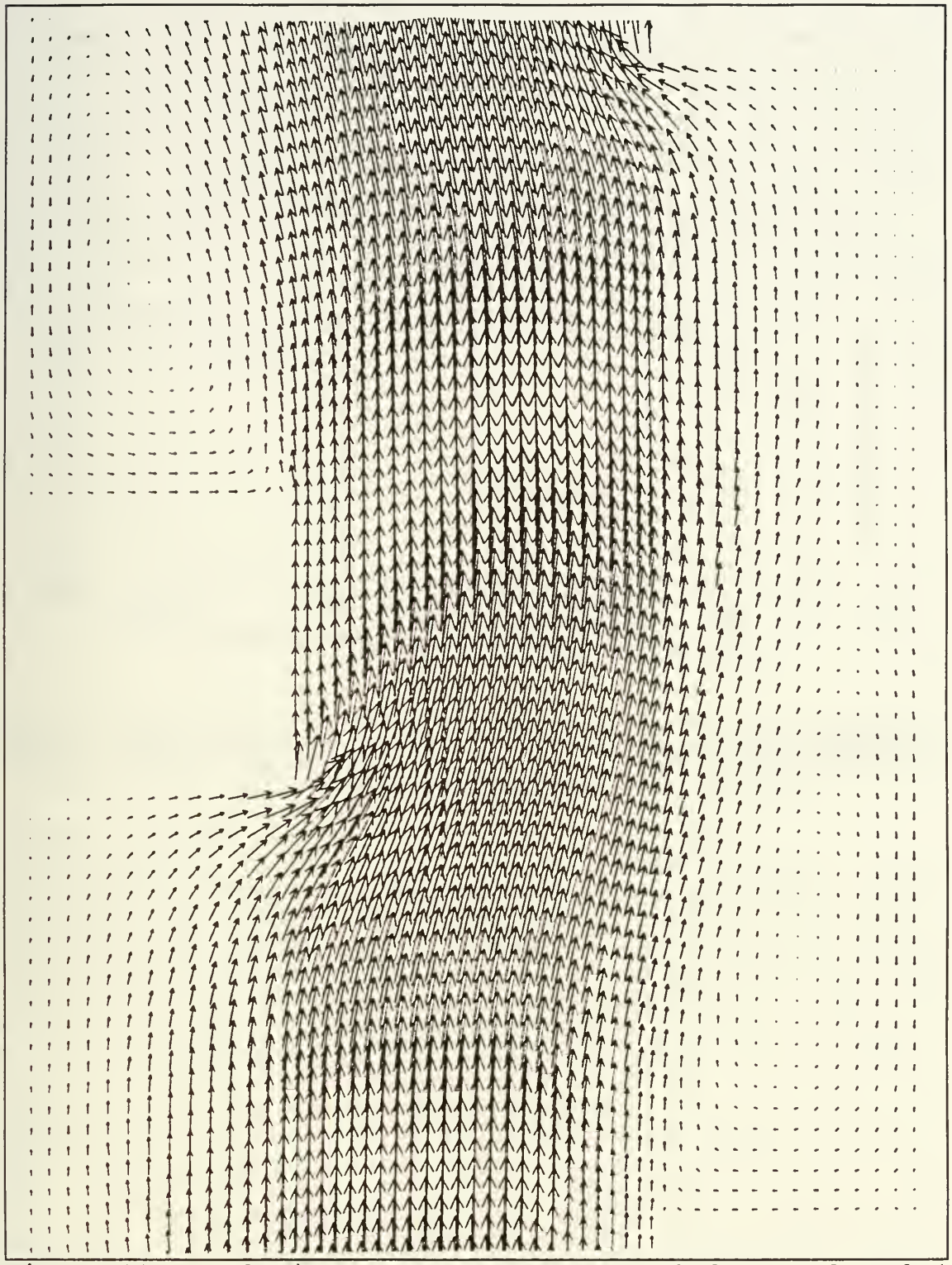

Figure 11 - Velocity Vectors Between Turbulators 2 and 4 Using a Constant Grid Spacing

reattachment point establishing a recirculation zone downstream of the turbulator. The flow then turns toward the next downstream turbulator. On the upstream face of this turbulator no recirculation occurs and the flow proceeds over the top with no separation on the upper surface.

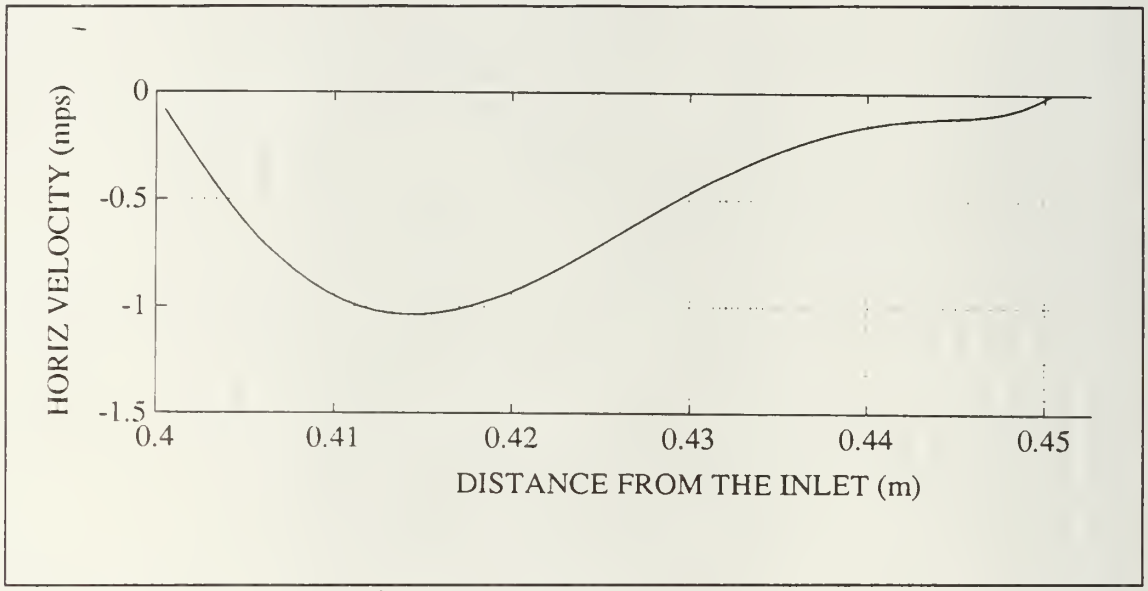

Figure 12 - Horizontal Velocity Component Between Turbulators 2 and 4 Using a Constant Grid Spacing

Using data generated in the Phoenics results files, the area between the eighth and tenth turbulators was investigated further. Figures 13 and 14 show the horizontal and vertical velocity components respectively of the flow in this area along the first grid line off the bottom wall. The horizontal velocity shows a minimum value of -0.51 m/s in the recirculation zone with the reattachment point located 0.014m downstream of the turbulator. The flow accelerates for 0.027m where it reaches a maximum of 1.9 m/s. After the reattachment

point all values for the flow are positive, verifying the lack of a recirculation region on the face of the tenth turbulator.

Figure 14 illustrates the vertical velocity component's maximum values are located in those areas immediately after and immediately prior to the turbulator faces.

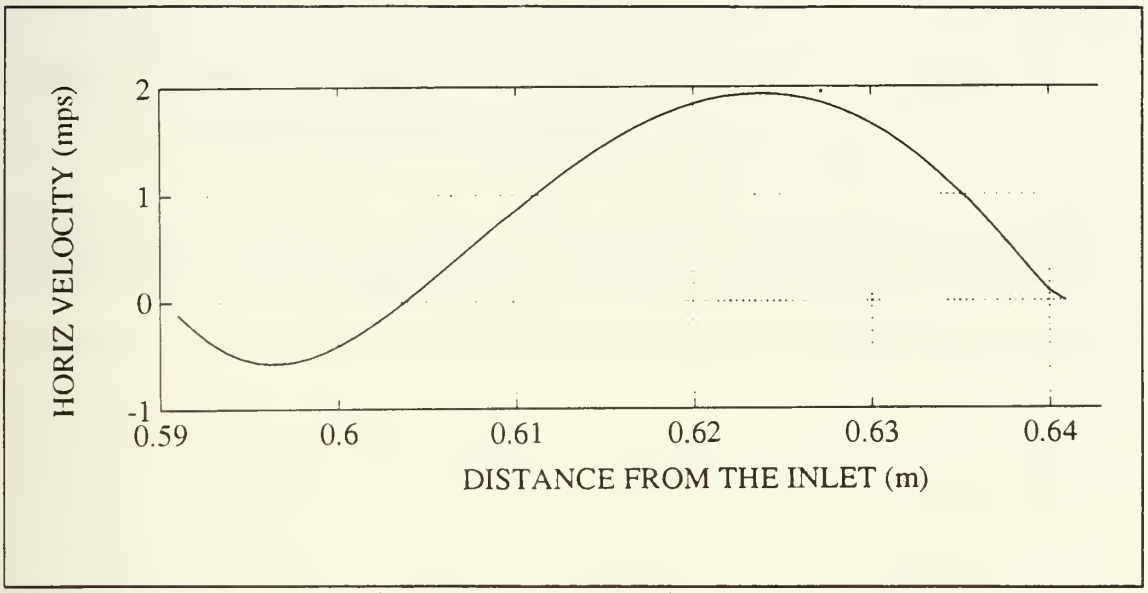

Figure 13 - Horizontal Velocity Component Between Turbulators 8 and 10 Using a Constant Grid Spacing

Figure 15 shows a plot of the calculated Stanton number versus location in the duct. The first peak is located adjacent to the downstream face of turbulator eight and coincides with the maximum vertical component of flow and a near zero value of horizontal velocity. Due to the location of this peak adjacent to the wall of the turbulator, predictions of global heat transfer were not consistent with those found in the experiment. This will be examined closer in the next section using grid stretching to cluster more grids near the wall.

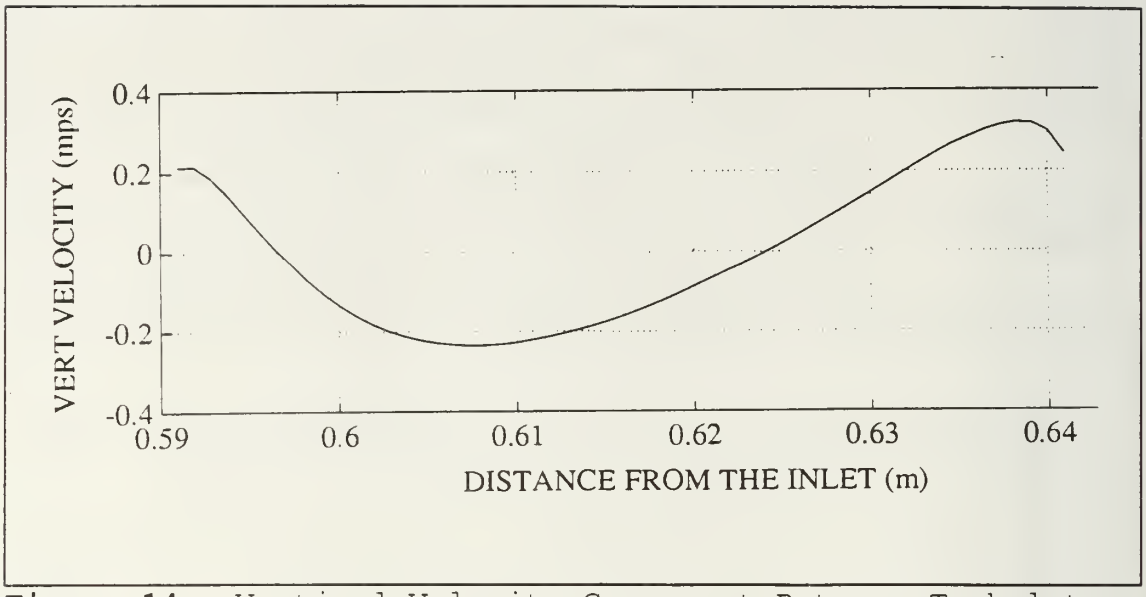

Figure 14 - Vertical Velocity Component Between Turbulators 8 and 10 Using a Constant Grid Spacing

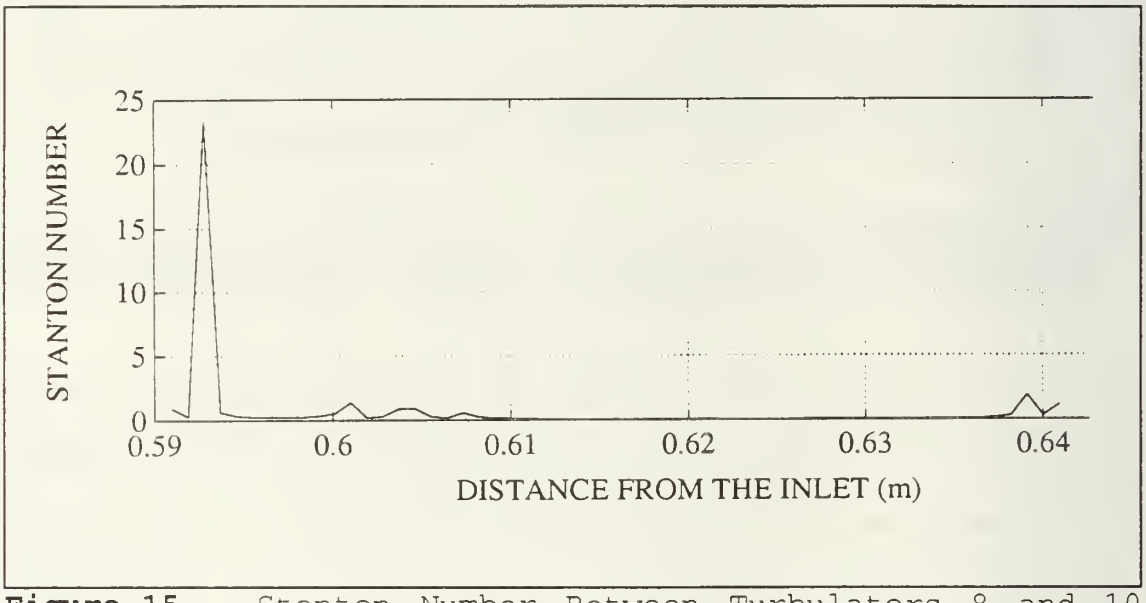

Figure 15 - Stanton Number Between Turbulators 8 and 10 Using a Constant Grid Spacing

The next three peak Stanton numbers occur between 0.010m and 0.011m from the downstream face of the turbulator. When compared to the velocity component plots, two distinct peaks are found to straddle the reattachment point with one

rather elongated peak occurring over the reattachment zone. The final peak occurs near the upstream face of the tenth turbulator. This maximum is located at the position of the maximum vertical component of the flow and where the horizontal component is nearing zero.

The effect of the fluid flow and heat transfer within the duct is shown in Figure 16 which is a plot of the wall temperature between the two turbulators. The maximum temperature develops near the downstream face of the eighth turbulator. The temperature first decreases and then increases to a relative maximum prior to the reattachment point.

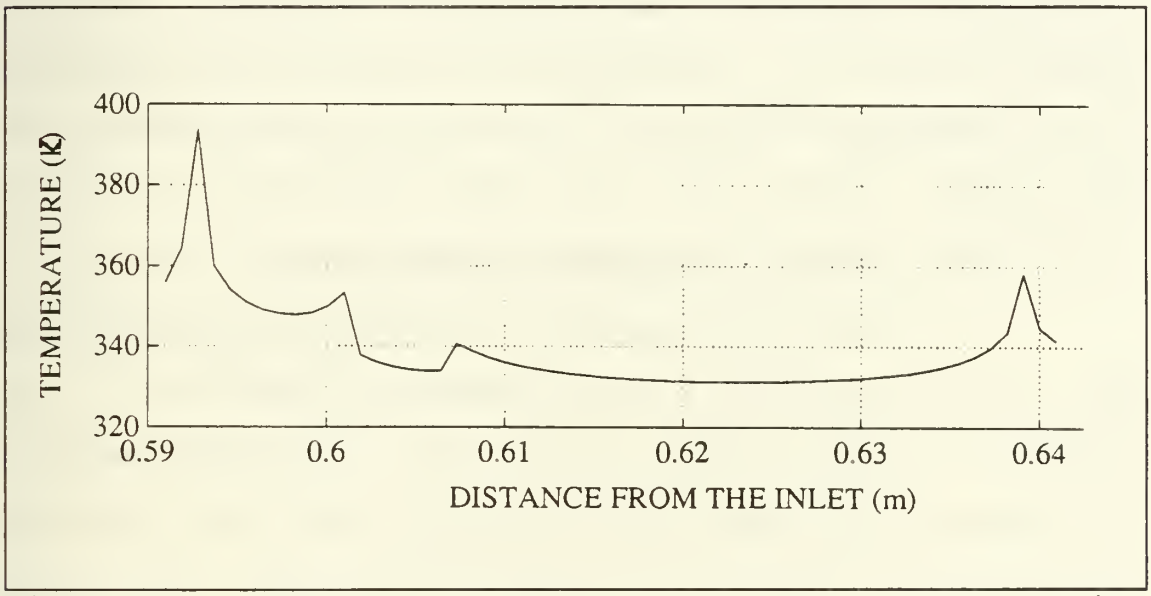

Figure 16 - Temperature Between Turbulators 8 and 10 Using a Constant Grid Spacing

At the reattachment point a relative minimum temperature results from the predominantly downward flow. Another relative

maximum occurs on the downstream side of the reattachment point followed by the minimum temperature region. This region corresponds to the area where the horizontal velocity component is, in general, one order of magnitude greater than the vertical component. A relative temperature maximum arises near the upstream face of the tenth turbulator, corresponding to the relative Stanton number maximum in the same location.

The development of the kinetic energy of turbulence is plotted in Figure 17. An initial decrease in the unturbulated area of the duct approaches a minimum of 4.3 X 10^{-2}. As the flow enters the turbulated region the effects of each turbulator is observed. The characteristic increases experienced by KE at each turbulator initially are on the order of 3.5 to 4.0. Eventually they decline to approximately 0.1. The total increase of KE approximates two orders of magnitude.

b. Simulation Using Grid Stretching

Using the same duct as above but with a 1.2 factor to stretch the grid in all regions in both the x and y direction, another simulation was run. Again the flow was run at a Reynolds number of 10000 with an inlet turbulence intensity of 2.0%. The initial development of the flow remained the same. The characteristic recirculation regions formed prior to both turbulators one and two. The area between turbulators two and four again contained totally

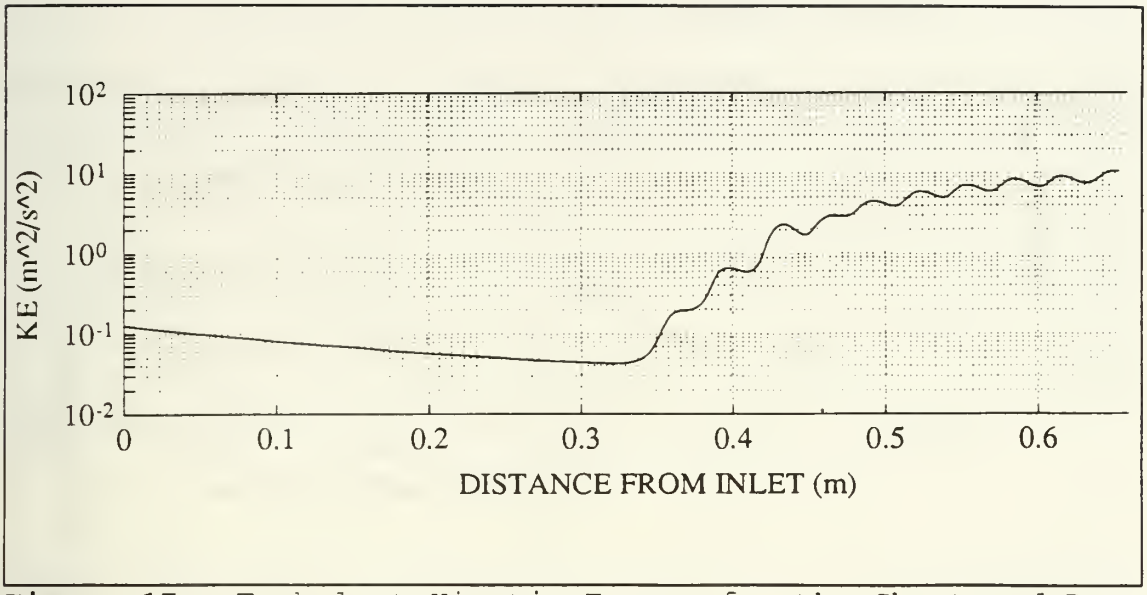

Figure 17 - Turbulent Kinetic Energy for the Shortened Duct

separated flow with no reattachment point. Subsequent flow developed in a pattern similar to the flow associated with a uniformly spaced grid. A reattachment point developed after the turbulator with an area of recirculation upstream of it between the turbulator and the reattachment point. No recirculation on the upstream face occurred for any flow after the second turbulator.

Again using the Phoenics results file the area between turbulators eight and ten can be examined closely. Figures 18 and 19 show the horizontal and vertical components of the flow velocity respectively in the analyzed regions. Figure 18 indicates this grid generated a larger recirculation zone than the uniformly spaced grid. The stretched grid developed a recirculation zone of 0.017m versus the uniform grid's 0.014m. The stretched grid also generated smaller

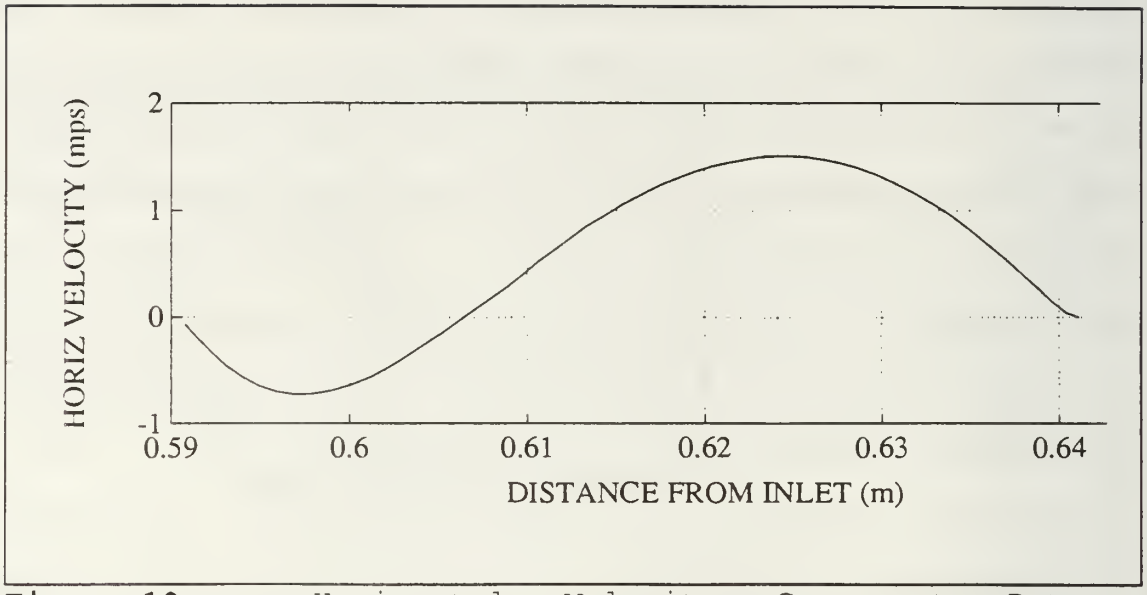

Figure 18 - Horizontal Velocity Component Between Turbulators 8 and 10 Using a 1.20 Stretching Factor

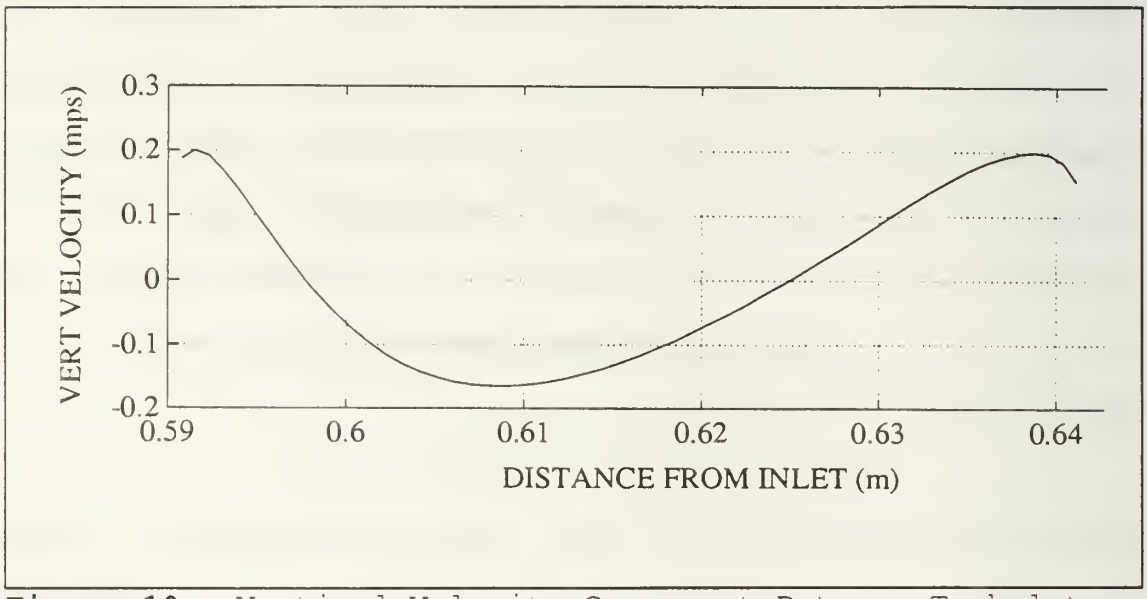

Figure 19 - Vertical Velocity Component Between Turbulators 8 and 10 Using a 1.20 Stretching Factor

maximum and minimum values for the vertical component of the velocity although the locations were relatively similar.

The plot of the Stanton number between the two turbulators (Figure 20) showed considerable differences when coupled with the one for the uniform grid (Figure 15).

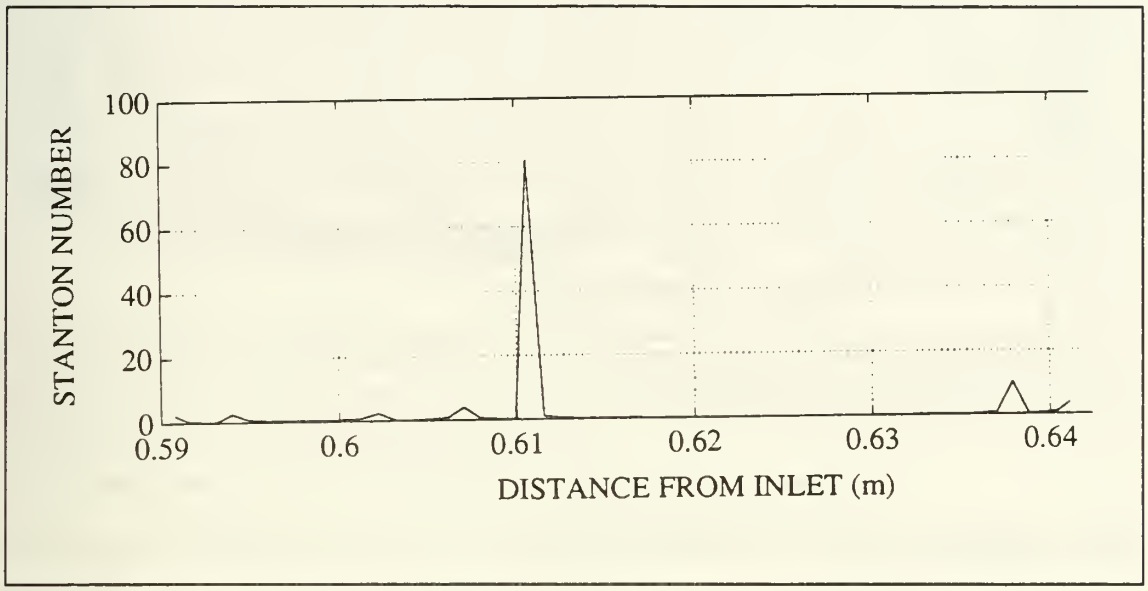

Figure 20 - Stanton Number Between Turbulators 8 and 10 Using a 1.20 Stretching Factor

The stretched grid solution located a relative maximum adjacent to the downstream face where the vertical component of the velocity was a maximum, and the horizontal component was near zero. It also located two relative maximums on either side of the reattachment point as determined from Figure 16. The next point identified is the maximum for the Stanton number in the area between these two turbulators. It is positioned just downstream from the minimum vertical velocity component, approximately 0.021m from the downstream face of turbulator 8. Its effect is discernable from Figure 21, the plot of the temperature distribution between the two turbulators.

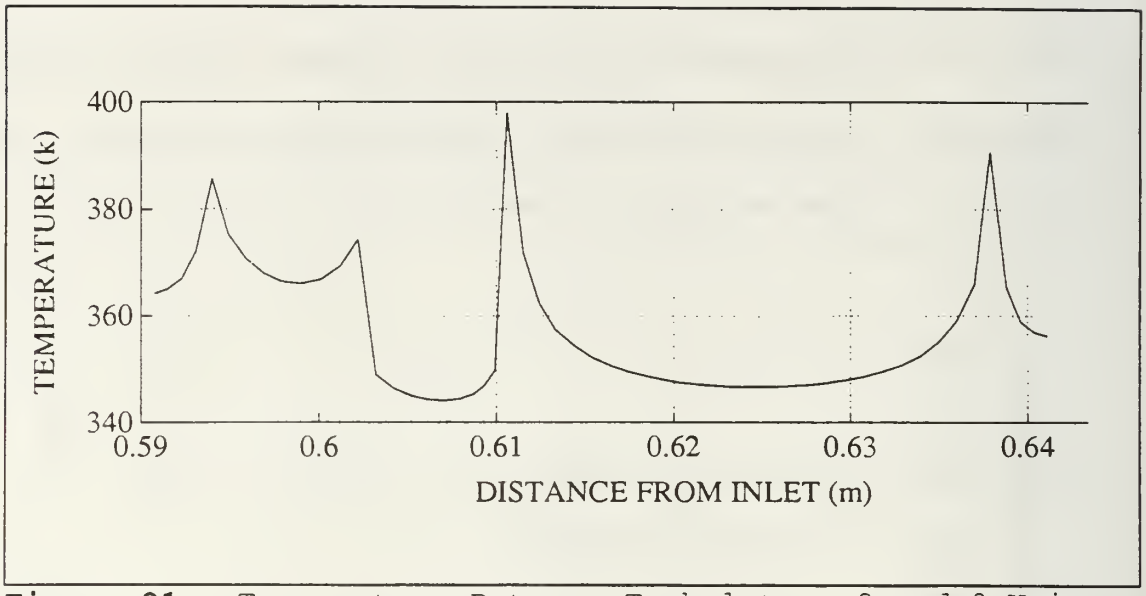

Figure 21 - Temperature Between Turbulators 8 and 9 Using a 1.20 Stretching Factor

The maximum temperature is located precisely where the maximum heat transfer occurs, as indicated by the Stanton number. The final relative peak for the Stanton number is located proximate to the upstream face of the tenth turbulator. As in the previous solution it is collocated with the maximum value for the flow's vertical component of velocity and where the horizontal component is approaching zero.

Since the maximum Stanton number and temperature occurs near the position on the grid where the clustering of the grid points for the upper turbulator is greatest, it appears that this maximum is grid related, rather than a valid depiction of the actual situation. Another variation of this configuration was run using a grid stretching factor of 1.10. As seen in Figure 22, the peak appearing in Figure 20 is not present for this new configuration. The new peak is located

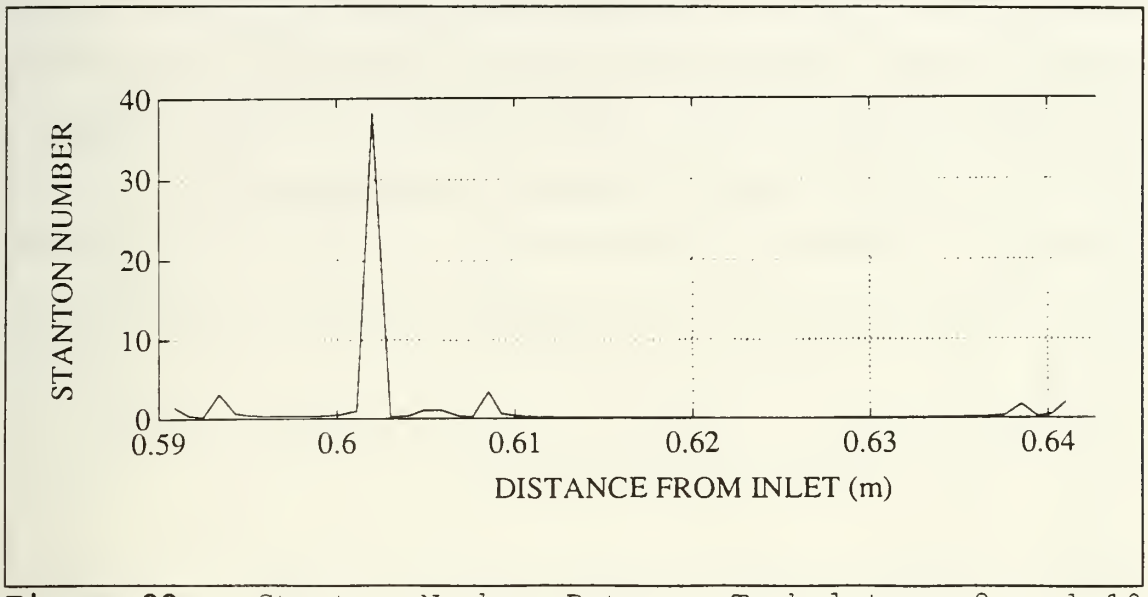

Figure 22 - Stanton Number Between Turbulators 8 and 10 Using a 1.10 Stretching Factor

on the upstream side of the attachment point and is half the magnitude of that experienced for a stretching of 1.20.

A final attempt to examine this grid generated anomaly was made using a grid stretching factor of 1.05. While this tended to cluster the grid closer to the downstream face of the turbulator, which appeared to rectify the spike from the uniformly spaced grid, it did not create an artificial spike in the area adjacent to or in the reattachment zone. Figure 23 is the Stanton number plot for the flow between turbulators eight and ten for this grid configuration. The most obvious difference between this and the previous cases is the reduction in the magnitudes of the peaks. All the peaks in this plot which are located at the same approximate location as the peaks associated with the previous grids are lower by an order of magnitude. The peak adjacent to the

downstream face of the turbulator is also approximately an order of magnitude smaller than the peak associated with the uniformly spaced grid. This analysis confirms that the solution for this area is highly grid dependent.

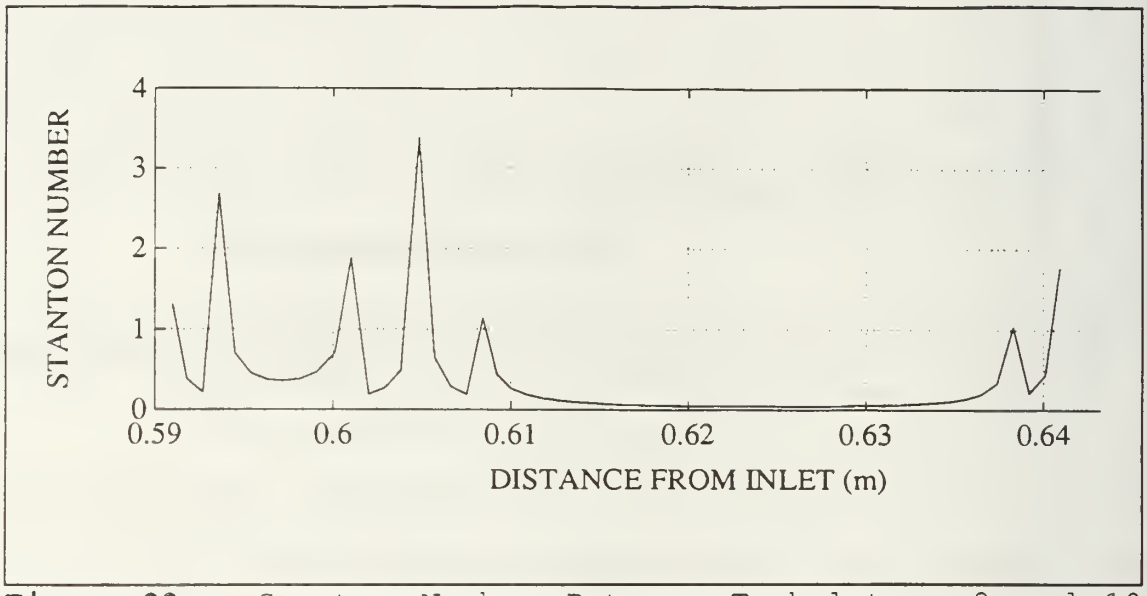

Figure 23 - Stanton Number Between Turbulators 8 and 10 Using a 1.05 Stretching Factor

The plot of the temperature for the area between turbulators eight and ten using a 1.05 stretching factor (Figure 24) shows that the maximum temperature is associated with the relative maximum Stanton number adjacent to the downstream face of the turbulator. The other three relative maximums for temperature are also associated with relative maximums of the Stanton number. Contrary to all previous investigations a relative minimum of the temperature occurs at a relative maximum Stanton number.

Defining shear stress according to equation 13 and plotting it for this portion of the duct results in Figure 25.

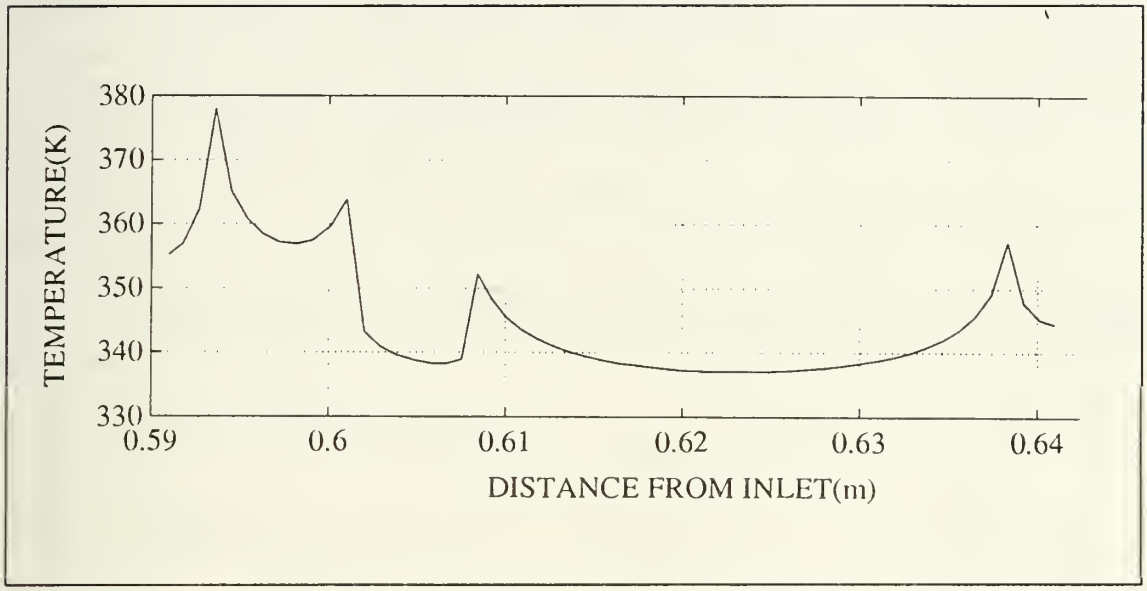

Figure 24 - Temperature Between Turbulators 8 and 10 Using a 1.05 Stretching Factor

Here the plot shows that the value of the shear stress at the point of the relative maximum Stanton number is zero.

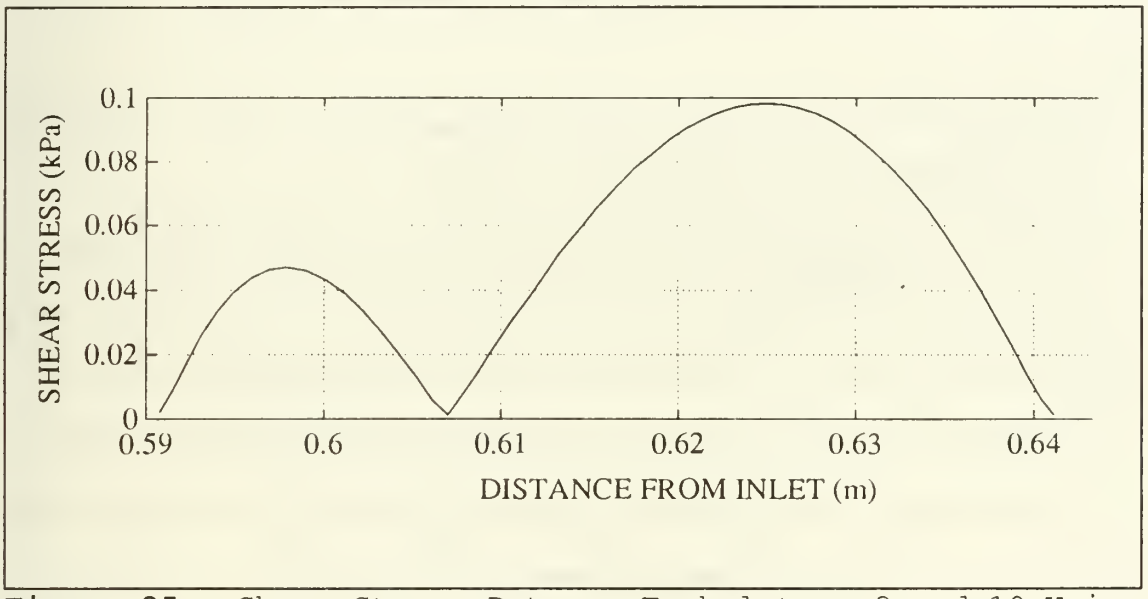

Figure 25 - Shear Stress Between Turbulators 8 and 10 Using a 1.05 Stretching Factor

This duct's turbulent kinetic energy plot (Figure 26) is very similar to that for the previous duct. Original

values are the same with the same initial decrease experienced. Although they both reached the same level of turbulence, the stretched grid appears to take longer to develop this value. The final increases, however, are still more than an order of magnitude smaller than the initial ones and can be considered to be an asymptotic condition.

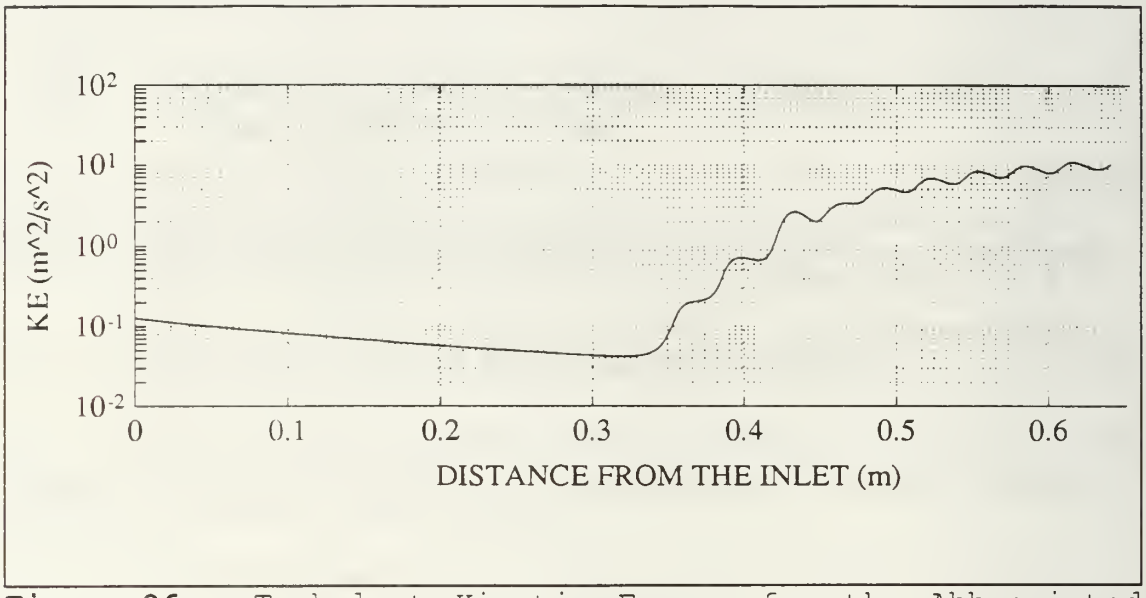

Figure 26 - Turbulent Kinetic Energy for the Abbreviated Duct Using a 1.05 Stretching Factor

Another investigation which was done was the determination of the effects of varying the turbulence intensity at the inlet. Figures 27 and 28 show plots of the KE at a mid-duct location for a Reynolds number of 20000 with the initial turbulence intensity being 2.0% and 0.5% respectively. As expected the starting and development areas of the duct for both conditions are different. However once the flow enters into the turbulated area, the flow patterns and the levels of turbulence start to converge. From this it can be concluded

that the level of turbulent kinetic energy at an asymptotic location in a duct is unaffected by the level of turbulence intensity far upstream.

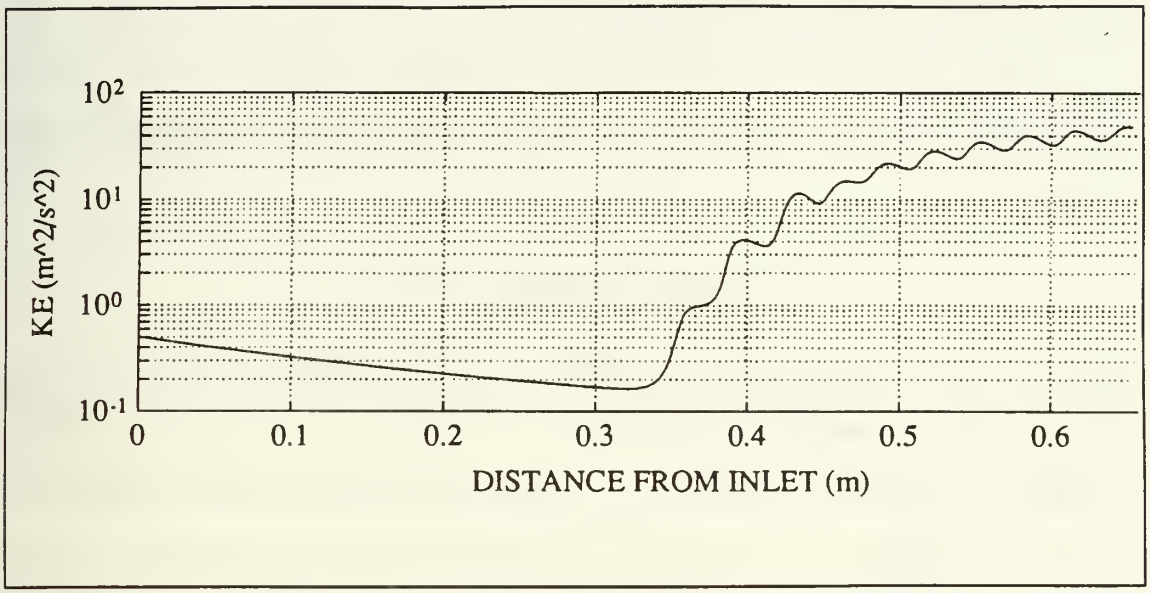

Figure 27 - Turbulent Kinetic Energy for a Reynolds Number of 2000 and a Turbulence Intensity of 2%

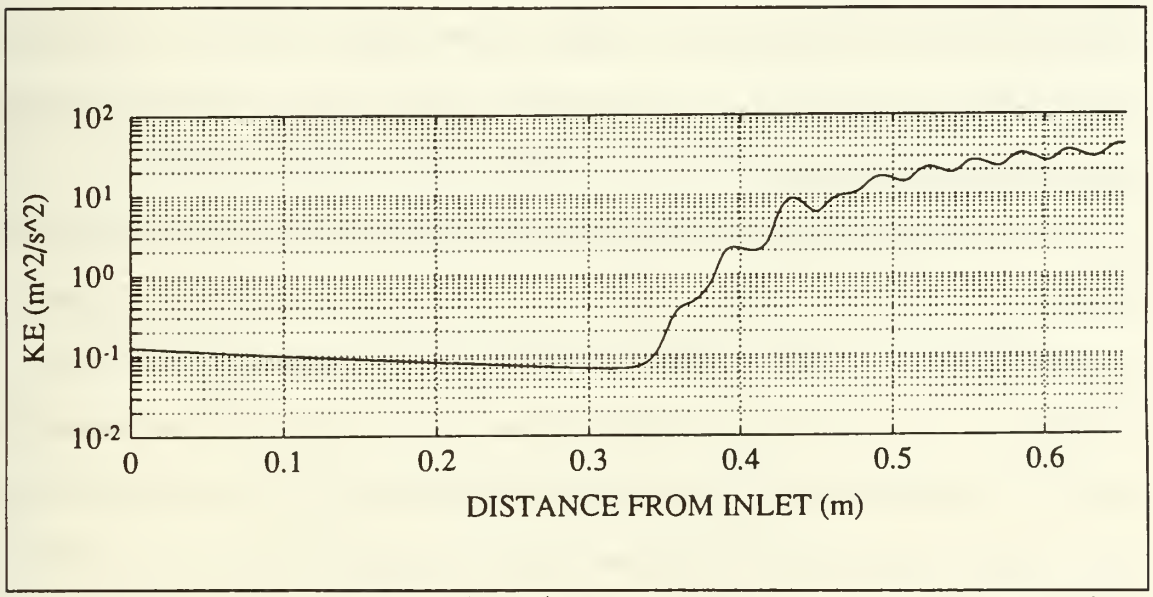

Figure 28 - Turbulent Kinetic Energy for a Reynolds Number of 20000 and a Turbulence Intensity of 0.5%

VI. COMPARISON OF RESULTS WITH EXPERIMENT

A. UNTURBULATED SQUARE DUCT

The results of the unturbulated square duct can be compared with the results of the Dittus-Boelter equation which states

$$Nu = 0.0243 Pr^{0.4} Re^{0.8} \quad (31)$$

where Nu is the Nusselt number. This equation is valid when the Prandtl number is between 0.7 and 160.0 and the Reynolds number is greater than 10^4. From Phoenics, the steady state Stanton number was calculated for Reynolds numbers of 10000 and 20000. This is a measure of the heat transfer occurring at the bottom wall of the duct. This number was then converted to the Nusselt number. Figure 29 is a plot of the Dittus-Boelter equation (dashed line) and the experimental data between Reynolds numbers of 10000 and 20000.

The disagreement between the Phoenics generated values for Nusselt number and the Dittus-Boelter correlation is considerable. The slope is opposite between the two and the magnitude is one full order higher for the Phoenics generated data. Operating at the lower end of the effective region for the Dittus-Boelter correlation and grid resolution problems are possible causes of this discrepancy.

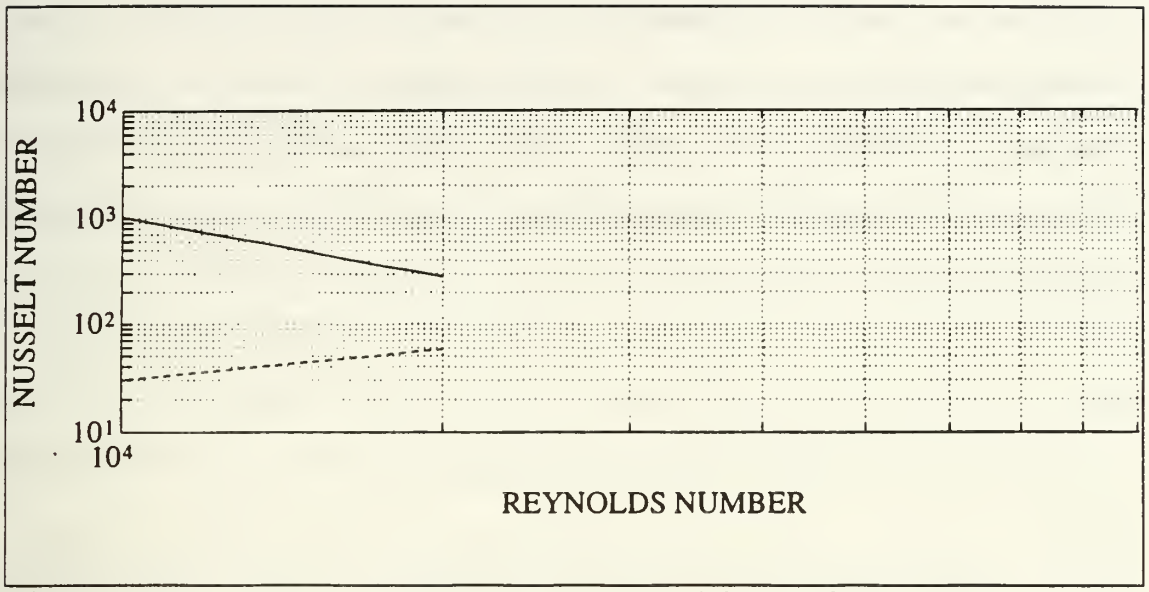

Figure 29 - Nusselt Number vs Reynolds Number for a Square Duct

B. TURBULATED RECTANGULAR DUCT

1. Constant Grid Spacing

The plot of the Stanton number for the uniformly spaced grid at a Reynolds number of 10000 (Figure 15) is dominated by the peak near the downstream wall. This is specific to this test case and does not appear on the plots for Reynolds numbers of 15000 or 20000. This adversely affects the entire slope of the numerically generated Nusselt number solutions.

Since each grid is a constant width, the average Stanton number over the entire zone can be resolved by determining the value for the Stanton number at each grid point and averaging it. Plotted on log-log paper with the results of Taslim and Spring [Ref 7], the results of the uniformly spaced grid show a negative slope, while that of the experimentally

generated data is positive. In addition, the experimental data corresponds closely to the slope of the Dittus-Boelter correlation line. A plot of these two lines is shown in Figure 30 with the experimental data being depicted with a dashed line.

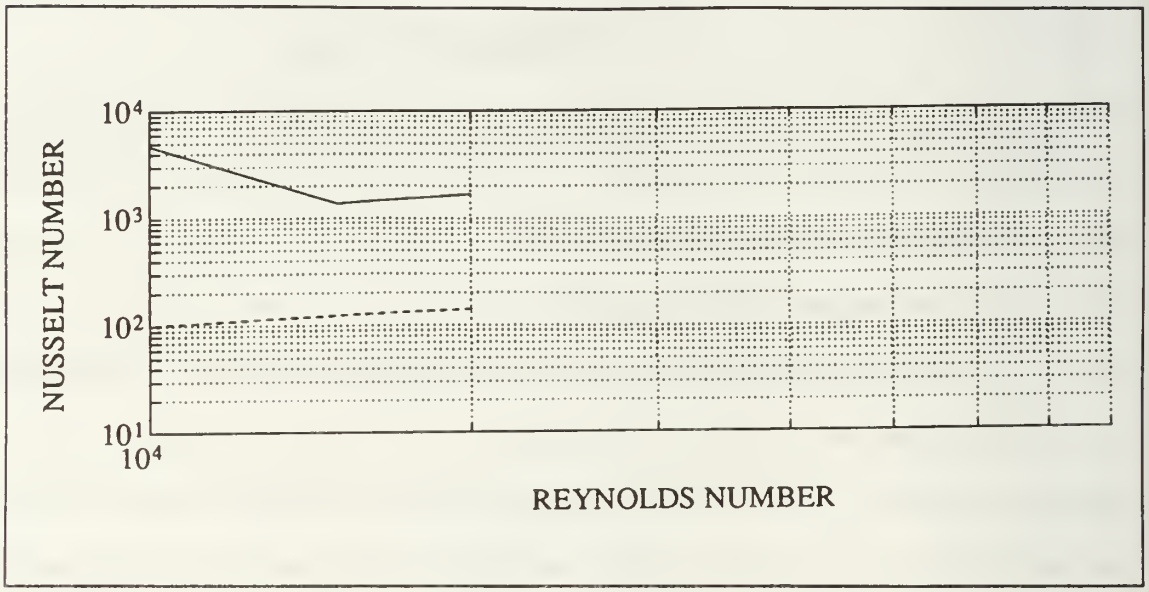

Figure 30 - Nusselt Number vs Reynolds Number for a Uniformly Spaced Grid

2. Grid Spacing Using Stretching

Three different factors of stretching were used throughout this analysis: 1.20, 1.10 and 1.05. Since the grids are variably spaced, the average Stanton number requires each individual Stanton number be multiplied by the width of its grid. All of these values must then be added together and then divided by the total width to determine the average.

The plots of the Stanton numbers of the 1.20 and 1.10 stretched grids are dominated by exceeding high artificial peaks (Figures 20 and 22). When converted to Nusselt numbers, averaged with the other values and plotted against Reynolds numbers, these artificially high values induce negative slopes on the resulting curves. This runs contrary to not only the results of Taslim, but also the Dittus-Boelter correlation and the Colburn correlation which states $Nu=f/2Pr^{1/3}Re$ where f/2 is a dimensionless shear stress term [Ref 36]. All of these clearly indicate an increase of Reynolds number should cause an increase of Nusselt number. A plot of the resultant graph for the stretching of the grid by factors of 1.10 and 1.20 are shown in Figures 31 and 32 respectively.

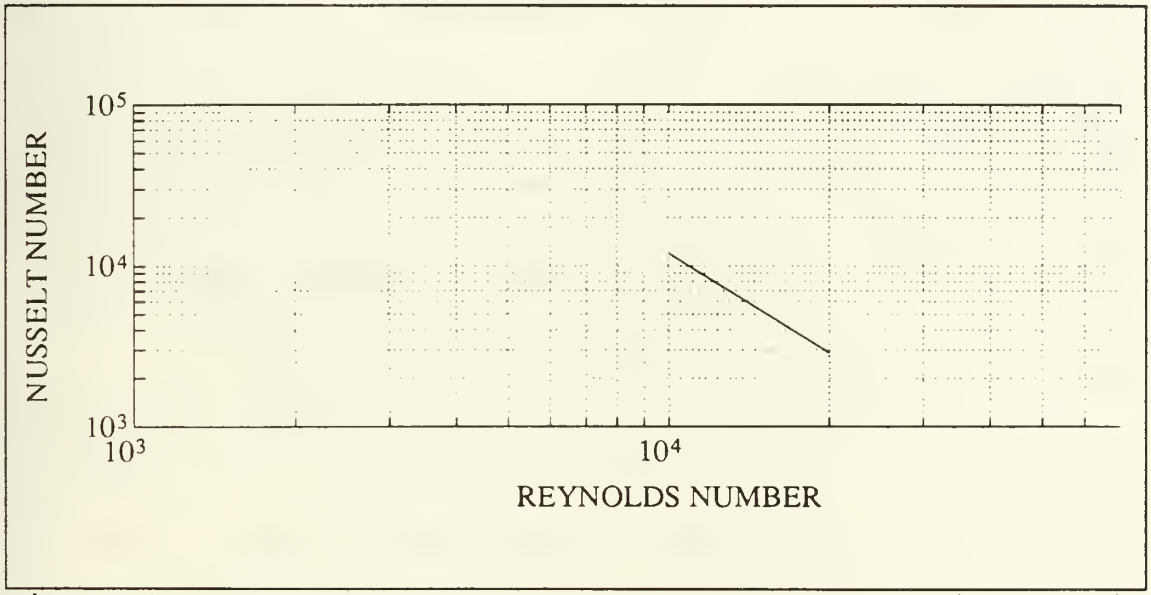

Figure 31 - Nusselt Number vs Reynolds Number Using a Grid Stretching Factor of 1.10

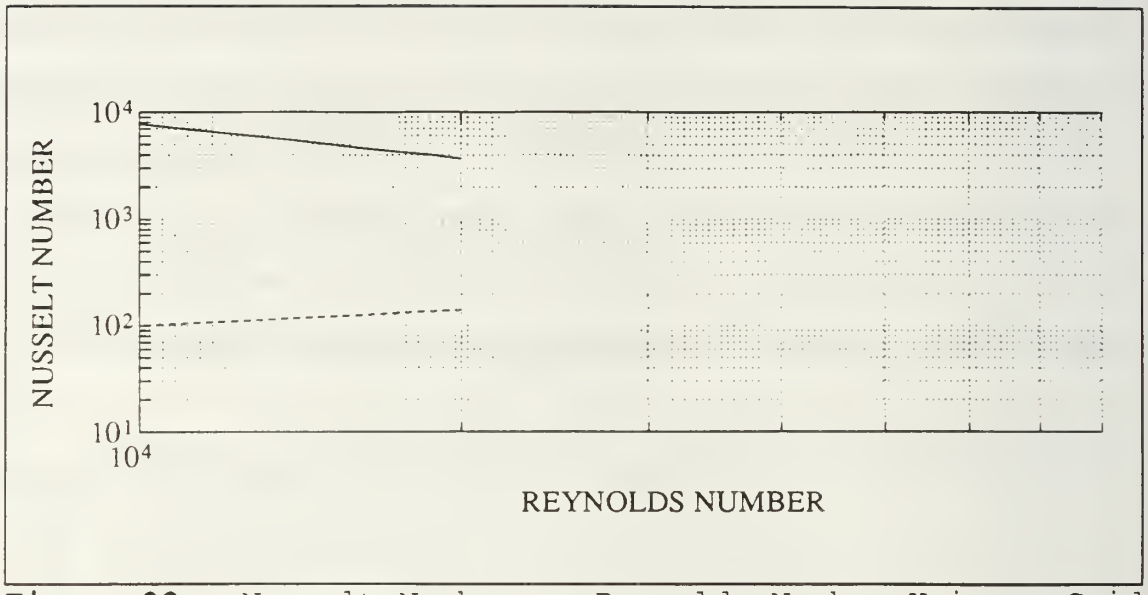

Figure 32 - Nusselt Number vs Reynolds Number Using a Grid Stretching Factor of 1.20

The stretching factor of 1.05 produced no such anomalies. The values for Stanton number were more consistent, with no one peak exceeding the others by an order of magnitude or more. The plot of this resultant curve is not similar to the slope of that generated by Taslim and Spring. As seen in Figure 33, with its minimal slope, it more closely approximates a constant Stanton number instead of an increasing one with increasing Reynolds number.

The calculation of the Stanton number by the Phoenics algorithm is a blind operation which does not reveal the equations or values used. To determine if the variance in the Phoenics generated Nusselt numbers are the result of a grid resolution problem, the Nusselt number was hand calculated

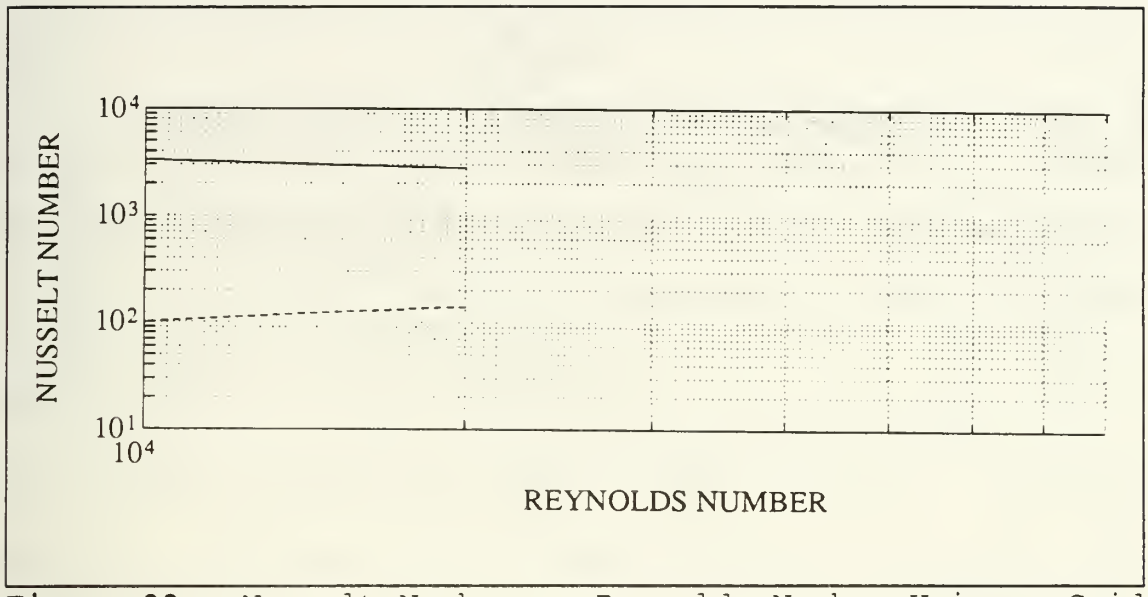

Figure 33 - Nusselt Number vs Reynolds Number Using a Grid Stretching Value of 1.05

from the values of component variables output by Phoenics and compared with the values computed in the code.

First the heat flux, q_0'', is defined as

$$q_0'' = (K + \rho \frac{C_\mu C_p k^2}{\sigma_t \epsilon}) \frac{\partial T}{\partial y} \qquad (32)$$

where K is the thermal conductivity of air at 300°K, C_μ is a constant in the k-ε turbulence model equal to 0.09, C_p is the specific heat of air at constant pressure and σ_t is the turbulent Prandtl or Schmidt number [Ref 37].

Once the value of the heat flux is determined, a local heat-transfer coefficient, h_x, is specified as

$$h_x = \frac{q_0''}{t_0 - t_\infty} \tag{33}$$

where t_0 is the specified temperature at the bottom wall. The t_∞ temperature is located at mid-duct. Finally the local Nusselt number can be generated from

$$Nu = \frac{h_x\, x}{K} \tag{34}$$

Here the x value is taken as the width of the cell for which the temperature, kinetic energy and dissipation of turbulence are being considered.[Ref 38]

A plot of the calculated Nusselt number versus the distance from the inlet is shown in Figure 34. The dashed line plot is the Phoenics generated values. A very striking resemblance exists between the two graphs. All but one of the maximums from the Phoenics results are identifiable for the calculated values. The one value which does not appear on the chart of the calculated values is the spike at the reattachment point. The indication is this spike is grid generated.

As a final comparison, the values for the average calculated Nusselt numbers for Reynolds numbers of 10000 and 20000 were plotted versus these Reynolds numbers in Figure 35. Also plotted were the values obtained from Phoenics for a 1.05 stretching factor solution (solid line) and the experimental values (dashed and dotted line). The slope for the calculated

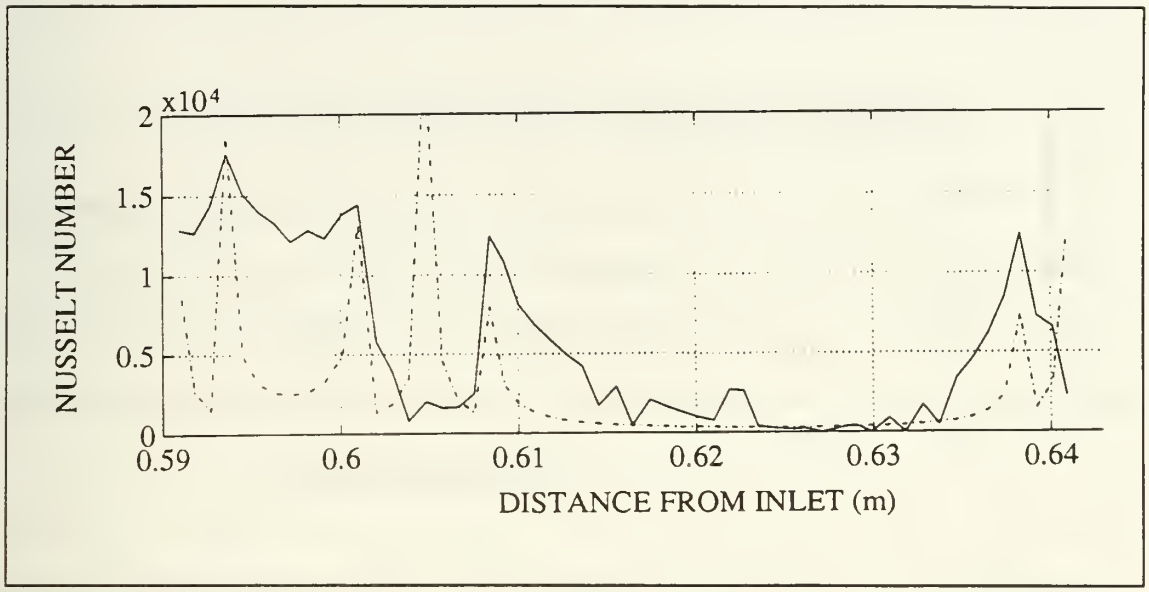

Figure 34 - Calculated and Phoenics Generated Values for Nusselt Number Between Turbulators 8 and 10

values is much closer to the experiment than that produced by Phoenics, but the magnitude is much greater.

Because of the close correlation between the Phoenics generated program and the hand calculated one, the failure to produce Taslim's results over a range of Reynolds numbers occurs due to an inability to adequately resolve the flowfield with this grid size.

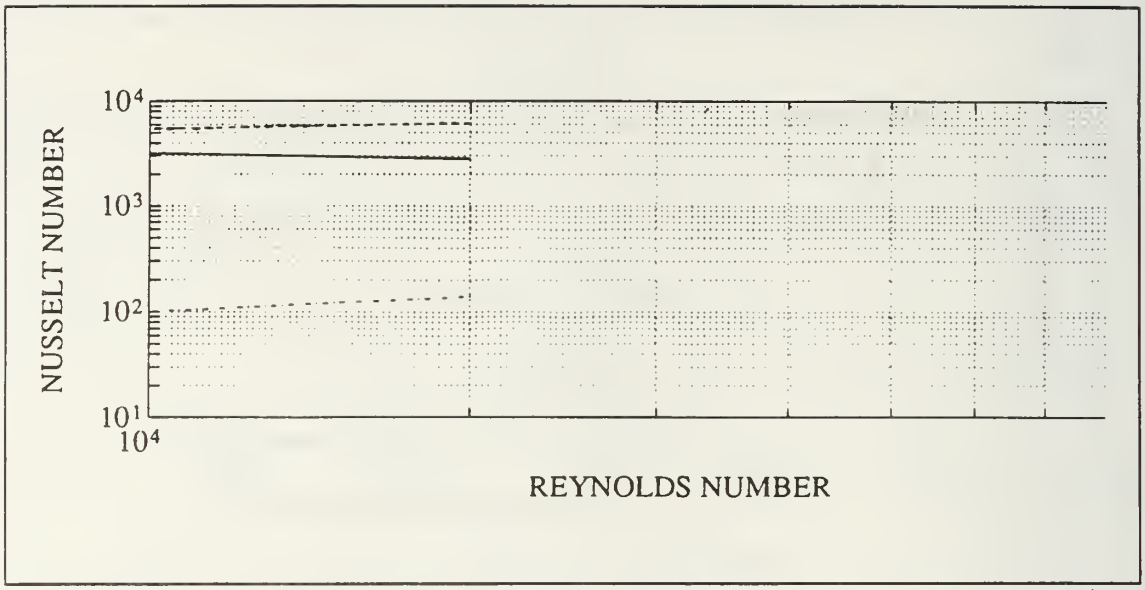

Figure 35 - Nusselt Number vs Reynolds Number Using Calculated, Phoenics Generated or Experimental Values

VII. CONCLUSIONS AND RECOMMENDATIONS

A. CONCLUSIONS

The analysis of the data presented in this investigation leads to a number of conclusions about airflow in a rectangular duct with square turbulators placed in a staggered array. Using a S/e ratio of 5, an e/D_h of 0.235, an AR_t of 1.0 (Taslim's value of D_h), with an e of 0.0127m, the following can be concluded:

- Flow approaching the first set of turbulators will experience recirculation on the upstream side of only the first pair of turbulators. All turbulators thereafter will direct the flow up and over the turbulator and will not generate a separation point for the recirculation of the oncoming flow.
- Flow over the top of the turbulators will remain attached and create no recirculation zones. This was true for a range of Reynolds numbers between 7000 and 30000 with turbulence intensity varying between 0.22 and 4.1.
- No reattachment point will develop for flow over the first or second turbulator. The entire region between turbulators two and four will be recirculating flow. This is the only area of the duct which will experience this flow structure.
- The pattern of flow between all sets of turbulators after the initial two on either wall will maintain the same characteristic structure. The flow will develop a recirculation region directly after the turbulator followed by a reattachment point. An area of acceleration of flow velocity toward the downstream turbulator will ensue with the flow traveling over the turbulator. Each succeeding section results in a smaller recirculation zone until an asymptotic dimension is reached.

- Maximum heat transfer occurs at the reattachment point of the downstream recirculation zone. In general four relative maximum heat transfer locations occur: on the downstream face of the turbulator, on either side of the reattachment point and on the upstream face of the following turbulator.

- The kinetic energy of turbulence throughout a turbulated duct maintains a distinct trace. Each turbulator increases the level as the medium passes over it. Initial turbulators provide a significantly greater level of increase than those located further along the duct. After eight turbulators, an asymptotic level of kinetic energy is reached.

- The asymptotic level of turbulence in a duct is independent of the turbulence intensity at the inlet. In this duct, the individual variation of kinetic energy caused by each turbulator increased or decreased with respect to a similar change in turbulence intensity. Thus altering the turbulence intensity did not change the results of the simulation.

- The detailed results are highly grid dependent. The choice of uniform or clustered grids not only effects the results, but the power of the clustering can also impact them. A converged solution can exhibit grid-generated phenomena which have no basis in actuality and for which the investigator must constantly inspect.

- This investigation was a 2-dimensional analysis of an experiment performed in three dimensions. The experimental results showed a variation in the spanwise direction of the duct. The effects of the walls on the flow caused lower values for the heat transfer coefficient near the sidewalls with an increase closer to the centerline. A 2-dimensional analysis would not have the effects of the sidewalls included and would produce this centerline higher value. This possibly explains the elevated values seen in the computed results.

B. RECOMMENDATIONS

Phoenics is a powerful program with the ability to solve highly complex flow problems. Its strength lies in the ease with which parameter can be altered and reevaluated for a given problem. The present analysis was done using strictly

a Cartesian coordinate system in two dimensions. With Phoenics' versatility an examination of alternative turbulator shapes and geometries is possible. Even the evaluation of the "jersey-barrier" shape in three dimensions is possible using body-fitted coordinates.

The non-linearity of the flow and the large number of equations which are solved required thousands of iterations for a converged solution. This can take an exceptionally long time even when operating on a 486-processor based computer. A 3000 iteration solution using the configuration of this report took 50 hours to complete.

Phoenics also requires the user to accept certain parameters and algorithms without the option to alter them. Although numerous areas are accessible, many of the turbulence parameters, wall functions and other built-in subroutines are not. This precludes making changes to fit the problem being examined.

A full analysis of a duct with any style turbulator should include a three dimensional examination of the flow. The 500 X 55 grid used here should be considered to be a minimum in two dimensions. The spanwise direction would add significantly more points in the grid and ultimately more equations to be solved. This will be excessively time consuming and may or may not provide the accuracy required.

For these reasons the recommendation of this report is to use Phoenics only for the first approximations of the solution

to the duct problem using coarse grids. The ease with which programs can be entered, changed and run makes it an excellent candidate for this type of initial investigation. It can locate areas of more increased flow activity and aid in the delineation of zones requiring clustered gridding. Several iterations with increasingly finer and more clustered grids will assist in either supporting or refuting the initial grid refinements.

Final analysis should be carried out using a program possessing at least as much power as Phoenics but with more flexibility and a faster running environment. Two such programs are Proteus 3-D and Overflow.

LIST OF REFERENCES

1. Cohen, H. Rogers, G.F.C., and Saravanamuttoo, H. I. H., *Gas Turbine Theory*, p. 232, Longman House, 1981.

2. Oates, G. C., *Aerothermodynamics of Aircraft Engine Components*, p. 278, American Institute of Aeronautics and Astronautics, 1985.

3. Wilkie, D., *Forced Convection Heat Transfer from Surfaces Roughened by Transverse Ribs*, paper presented at the Third International Heat Transfer Conference, Chicago, Illinois, 8 August 1966.

4. General Electric Research and Development Center Report #68-C-273, *The Effect of the Transverse-Rib Type of Roughness on Heat Transfer and Friction Factor for Turbulent Flow of Air in Ducts* by R. H. Norris, July 1968.

5. Han, J. C., Park, J. S., and Lei, C. K., "Heat Transfer Enhancement in Channels with Turbulence Promoters", *ASME Journal of Engineering for Gas Turbines and Power*, v. 107, pp. 628-635,1985.

6. Lau, S. C., McMillin, R. D., and Han, J. C., *Heat Transfer Characteristics of Turbulent Flow in a Square Channel with Angled Discrete Ribs*, ASME Report #90-GT-254, 1990.

7. Taslim, M. E., and Spring, S. D., *An Experimental Investigation into the Effects Turbulator Profile and Spacing Have on Heat Transfer Coefficients and Friction Factors in Small Cooled Turbine Airfoils*, AIAA Paper AIAA-91-2033, 1991.

8. NASA Technical Memorandum 83614, *Heat Transfer in Serpentine Passages with Turbulence Promoters*, by Robert J. Boyle, 1984.

9. Chandra, P. R., Han, J. C., and Lau, S. C., "Effect of Rib Angle on Local Heat/Mass Transfer Distribution in a Two-Pass Roughened Channel", *Journal of Turbomachinery*, v. 110, pp. 233-241, 1987.

10. Han, J. C., and Zhang, P., *Effect of Rib Angle Orientation on Local Mass Transfer Distribution in a*

Three-Pass Rib Roughened Channel, ASME Paper 89-GT-98, 1989.

11. Chyu, M. K., *Regional Heat Transfer and Pressure Drop in Two-Pass and Three-Pass Flow Passages with 180-Degree Sharp Turns*, ASME Paper 89-GT-191, 1989.

12. Han, J. C., and Zhang, P., *Effect of Rib Angle Orientation on Local Mass Transfer Distribution in a Three-Pass Rib Roughened Channel*, ASME Paper 89-GT-98, 1989.

13. AGARD Conference Proceedings #390, *Rotating Heat Transfer Investigations on a Multipass Cooling Geometry* by R. J. Clifford, pp 2-1 through 2-12, May 1985.

14. AGARD Conference Proceedings #390,*Local and Mean Heat Transfer on the Leading and Trailing Surfaces of a Square-Sectioned Duct Rotating in the Orthogonal Mode*, by W. D. Morris and S. P. Harasgama,pp. 3-1 - 3-12, May 1985.

15. Kheshi, H. S., and Scriven, L. E.,"Viscous Flow through a Rotating Square Channel", *Physics of Fluids*, v. 28, #10, pp. 2968-2978, 1985.

16. Harasgama, S. P. and Morris, W. D., "Influence of Rotation on the Heat Transfer Characteristics of Circular, Triangular and Square Sectioned Coolant Passages of Gas Turbine Rotor Blades", *ASME Journal of Turbomachinery*, v. 110, pp. 44-50, January 1988.

17. Meyer, R. E., *Introduction to Mathematical Fluid Dynamics*, pp. 134-136, Wiley-Interscience, 1971.

18. NASA Conference Publication 2493, *Turbine Engine Hot Section Technology*, by Hajek, T. J., Wagner, J. H., and Johnson, B. V., 1987.

19. Taslim, M. E., Rahman, A., and Spring, S. D., *An Experimental Investigation of Heat Transfer Coefficients in a Spanwise Rotating Channel with Two Opposite Rib-Roughened Walls*, ASME Paper 89-GT-150, 1989.

20. Guidez, J., "Study of the convective Heat Transfer in a Rotating Coolant Channel", *ASME Journal of Turbomachinery*, v 111, pp 43-50, January 1989.

21. Wagner, J. H., Johnson, B. V., and Kopper, F. C., *Heat Transfer in Rotating Serpentine Passages with Smooth Walls*, ASME Paper 90-GT-331, 1990.

22. Morris, W. D., and Hanami-Nasr, G. G., *Heat Transfer Measurements in Rectangular Channels with Orthogonal Mode Rotation*, ASME Paper 90-GT-138, 1990.

23. Taslim, M. E., Chrysafis, C., and Kercher, D. M., "An Experimental Study of Heat Transfer in a Spanwise Rotating Channel Turbulated with 45 Degree Criss-Cross Ribs", a paper presented at the ASME WAM 1989, San Francisco, CA, 1989.

24. Taslim, M. E., Bondi, L. A., and Kercher, D. M., "An Experimental Investigation of Heat Transfer in an Orthogonally Rotating Channel Roughened with 45 Degree Criss-Cross Ribs on Two Opposite Walls", a paper presented at the 1990 International Gas Turbine Conference, Brussels Belgium, 1990.

25. AGARD Conference Proceedings #510, *Numerical Representation of Heat Transfer in Turbine Blade Cooling Ducts*, by C. Taylor, J. Y. Xia, J. O. Medwell and W. D. Morris, pp. 6-1 - 6-12, July 1989.

26. AGARD Conference Proceedings #469, *Effects of Secondary Flow on Heat Transfer in Rotating Passages* by J. G. Moore and J. Moore, pp. 10-1 - 10-13, September 1989.

27. Medwell, J. O., Morris, W. D., Xia, J. Y, and Taylor, C., *An Investigation of Convective Heat Transfer in a Rotating Coolant Channel*, ASME Paper 90-GT-339, 1990.

28. Patankar, S. V., and Prakash, C., "Combined Free and Forced Convection in Vertical Tubes with Radial Internal Fins", *Journal of Heat Transfer*, v. 103, pp. 566, 1981.

29. Rowley, G.J. and Patankar, S. V., "Analysis of Laminar Flow and Heat Transfer in Tubes with Internal Circumferential Fins", *International Journal of Heat Mass Transfer*, v. 27, pp 553-564, 1984.

30. Patankar, S. V., Kelkar, K. M., "Numerical Predictions of Flow and Heat Transfer in a Parallel Plate Channel with Staggered Fins", *Journal of Heat Transfer*, v. 109, pp 25-30, 1987.

31. Schlicting, H., *Boundary Layer Theory*, 7th Edition, pp. 22-84, McGraw-Hill Book Co., Inc., 1979.

32. Anderson, D. A., Tannehill, J. C., and Pletcher, R. H., *Computational Fluid Mechanics and Heat Transfer*, p. 214, Hemisphere Publishing Corporation, 1984.

33. Launder, B. E. and Spalding, D. B., *The Numerical Computation of Turbulent Flows, Computation Methods of Applied Mechanical Engineering*, v. 3, pp. 269-289, 1974.

34. Patankar, S. V., *Numerical Heat Transfer and Fluid Flow*, p. 15, Hemisphere Publishing, 1980.

35. Patankar, S. V. and Spalding, D. B., "A Calculation Procedure for Heat, Mass and Momentum Transfer in Three-Dimensional Parabolic Flows", *Journal of Heat and Mass Transfer*, v. 15, pp 1787-1806, 1972.

36. Bejan, A., *Convection Heat Trasfer*, p. 265, John Wiley and Sons, Inc., 1984.

37. Rodi, W., "Examples of Turbulence-Model Applications", *Turbulence Models and Their Applications*, v. 2, pp. 297-298, 1984.

38. Kays, W. M., and Crawford, M. E., *Convective Heat and Mass Transfer*, 2d ed., p. 137, McGraw-Hill Book Company, 1980.

Initial Distribution List

		No. Copies
1.	Library, Code 0142 Naval Postgraduate School Monterey, California 93943-5002	2
2.	Defense Technical Information Center Cameron Station Alexandria, Virginia 22304-6145	2
3.	Department Chairman, Code AA Department of Aeronautics Naval Postgraduate School Monterey, California 93943	1
4.	Director, Turbopropulsion Laboratory Code AA/SF Department of Aeronautics Naval Postgraduate School Monterey, California 93943	10
5.	Naval Air Systems Command AIR-53616B (Attn: LCDR M. Johns) Washington, District of Columbia 20361-5360	1
6.	Naval Air Systems Command AIR-53616B (Attn: LCDR G. Selman) Washington, District of Columbia 20361-5360	1
7.	Naval Air Systems Command AIR-536T(Attn: Dr. L. Sloter) Washington, District of Columbia 20361-5360	1
8.	Naval Air Warfare Center Aircraft Division (Trenton) PE-31(Attn:S. Clauser) 250 Phillips Blvd Princeton Crossroads Trenton, New Jersey 08628-0176	1
9.	Commandant (G-EAE) 98-70098 United States Coast Guard 2100 Second Street, S.W. Washington, District of Columbia 20593-0001	2

10. Commandant (G-EAE-4) 1
Attn: CDR R. Renout
98-70098
United States Coast Guard
2100 Second Street, S.W.
Washington, District of Columbia 20593-0001

11. Admiral G.H. Smith 1
956 Rancho Circle
Fullerton, California 92635

Prof. M. E. Taslim 1
Associate Professor of
Mechanical Engineering
Northeastern University
Boston, Massachusetts 02115

12. LT Robert M. Palatka, USCG 2
504 Pershing Street
Ellwood City, Pennsylvania 16117